



Self-regulatory Fractional Fuzzy Control for Dynamic Systems: An Analytical Approach

Vijay Mohan¹ · Bharti Panjwani² · Himanshu Chhabra³ · Asha Rani⁴ · Vijander Singh⁴

Received: 8 April 2022 / Revised: 22 August 2022 / Accepted: 26 September 2022 / Published online: 8 November 2022
© The Author(s) 2022

Abstract This paper presents an analytical design of a fractional order fuzzy proportional integral plus derivative (FOFPI + D) controller. Artificial intelligence is incorporated into the controller with the help of a formula-based fuzzy logic system. The designed scheme combines fractional order fuzzy PI (FOFPI) and fractional order fuzzy D (FOFD) controller, derived from fundamental FOPID control law. The proposed scheme enjoys the linear structure of the FOPID controllers with non-linear gains that provide self-tuning control capability. The sufficient condition for stability of the closed-loop system is also established using the graphical approach. Performance of the proposed FOFPI + D, its integer order variant (FPI + D), and conventional controllers is examined for control of a highly non-linear and uncertain two-link robotic manipulator system. The optimum parameters of controllers are found by minimising aggregated control variation and error objective through non-dominated sorting genetic algorithm-II (NSGA-II). The comparison for trajectory tracking shows that FOFPI + D has the minimum integral absolute error (IAE) compared to other controllers. Further, rigorous performance investigations

are performed to verify the robustness of designed controllers against parametric uncertainties, the varying boundary conditions of reference trajectory and disturbance rejection. It is concluded from the results that the proposed FOFPI + D controller exhibits superior performance.

Keywords Self-regulatory control · Robust control · Fractional order fuzzy PID · Non-dominated sorted genetic algorithm-II

1 Introduction

Over the last decade, fractional calculus has emerged as one of the best innovative tools for modelling and controlling dynamic systems. Including fractional order (FO) operators in design adds an extra degree of freedom, providing flexibility and superior performance. Therefore, the application of fractional differ-integral operators in controllers has gained recent research thrust in the field of control of motor [1], renewable energy [2, 3], process control [4, 5], power system [6, 7], robotics [8–11], tumour growth control [12, 13], and automatic voltage regulation [14]. Moreover, it is widely utilised with advanced intelligent techniques for the design and control of real-world systems.

Intelligent techniques such as fuzzy logic and its variants have been effectively used in security design for the networked control system, autonomous vehicles, and control of time-varying, non-linear systems [15–18]. Fuzzy logic is the branch of artificial intelligence (AI) that provides excellent control of the uncertain and imprecise system through expert knowledge-based reasoning and cognitive abilities [19]. This feature motivated researchers

✉ Vijay Mohan
vijay.mohan@manipal.edu; vijay13787@gmail.com

¹ Department of Mechatronics, Manipal Institute of Technology, Manipal Academy of Higher Education, Manipal, Karnataka 576104, India

² Division of Instrumentation and Control Engineering, NSIT, University of Delhi, Delhi, India

³ Mechatronics Department, Parul University, Gujrat, Vadodara, India

⁴ ICE Division, Netaji Subhas University of Technology, New Delhi 110078, India

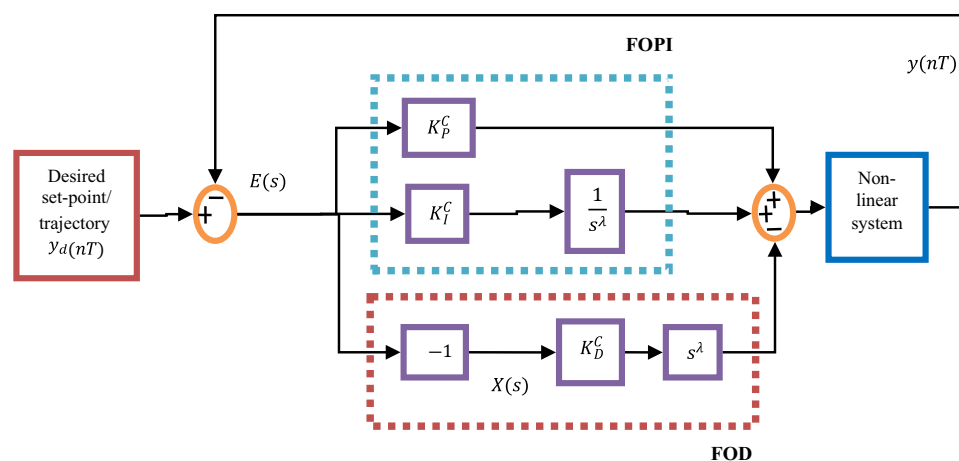


Fig. 1 Control schematic of FO PID controller

across the globe to incorporate fuzzy logic-based intelligence into conventional controllers and enhance its capabilities. Different fuzzy logic controller (FLC) structures based on classical proportional integral-derivative (PI/PD/PID) have been proposed in the literature. The controller design proposed in [20] is based on analytical formulae that provide self-tuning capability and preserve PI/PD/PID linear structure. The closed-loop system stability is analysed using the small gain theorem, and the bounded input bounded output (BIBO) stability condition is established [19–28].

In recent years, fuzzy logic-based linear PID controller performance has been improved by replacing integer order operators with fractional operators. Literature reveals the applicability of fractional FLC in the field of control problems [29–37]. Das et al. introduced the family of fractional order fuzzy PID controllers by utilising fractional differ-integral operators on error and control signals. Input and output scaling gains and fractional operators are optimised with a genetic algorithm, and their performance is compared for FO processes with dead time [29]. Das et al. also presented the application of FO fuzzy PID for control of the nuclear reactor and the unstable process. The controller design variables are tuned with the genetic algorithm, and its performance proved superior to conventional fuzzy PID controllers [30, 31]. A different type of fractional order fuzzy PD plus conventional I controller is proposed by Jesus et al. [32], in which a basic genetic algorithm is utilised to optimise its parameters. Due to efficient and robust control offered by fractional order fuzzy PID controllers, its implementation is found in diverse fields such as load frequency control of interconnected systems [33], smart seismic isolated structures [34], automatic generation control of power systems [35], hydrometallurgy [36], hybrid power system [37], bioreactor [38].

The above discussed fractional order fuzzy PID controllers are designed based on expert knowledge rather than the analytical method. Consequently, desirable properties of a controller such as controllability, stability, and reliability become significant concerns. Therefore, a design methodology based on the precise mathematical model of fractional order fuzzy controllers needs to be explored to deal with these problems. The present work aims to design the fractional order fuzzy controller by using fragmented fractional order PID control structure. A novel FO fuzzy PID (FOFPI + D) control law is derived mathematically from the conventional fractional order PID controller, exhibited in Fig. 1. The structure of FOFPI + D is the combination of FO fuzzy proportional-integral (FOFPI) and FO fuzzy derivative (FOFD) action. The designed scheme shows self-tuning control capability, as the gains vary nonlinearly besides retaining the properties and advantages of traditional non-integer PID controllers. The required BIBO stability conditions are analytically derived for the closed-loop system using two straight line method.

Further, the performance of the proposed control scheme is examined on the two-link robotic manipulator, which is non-linear and exhibits multi-input multi-output coupled behaviour. The parameters associated with membership functions, input and output scaling factors, and FO operators of the FOFPI + D controller are optimised with non-dominated sorting genetic algorithm-II (NSGA-II) for getting minimum variations in manipulating signal and sum of absolute error. The comprehensive simulation study is done to validate the robustness of the designed controller over its integer order counterpart for trajectory tracking, parametric uncertainties, tracking for varying boundary conditions of reference trajectory, and disturbance rejection. The results obtained demonstrate that the FO fuzzy PI + D controller performs better than its integer order equivalent in all case studies. Incorporating a non-integer

operator in design adds an extra degree of freedom, thereby providing better design performance over its integer order equivalent. The significant contribution of this work is summarised as.

1. Precise analytical formulae of the proposed FOFPI + D controller are derived from the FO PID controller. A mathematically derived simple fuzzy technique is fused with derived PID action to obtain intelligent and adaptive FOPID.
2. The proposed controller preserves the linearity of traditional FO PID and has self-tuning capabilities.
3. Stability requirements for the closed-loop control structure are ascertained methodically using the graphical approach.
4. The performance of the designed controllers is adequate and robust compared to its integer order equivalent while addressing different operating conditions such as parameter uncertainty, disturbance, and altering reference trajectory for the highly non-linear two-link robot.

The structure of the paper is as follows. A brief literature review is presented in Sect. 1 and the problem formulation is discussed in Sect. 2. The design methodology of FOFPI + D control, stability conditions, and the implementation of the NSGA-II algorithm are outlined in Sect. 3. The performance analysis of FOFPI + D for controlling the two-link robotic manipulator is presented in Sect. 4. This section also presents the comparative study of the proposed controller with its integer order variant for trajectory tracking, parametric uncertainty, and disturbance rejection. Finally, the concluding notes are discussed in Sect. 5.

2 Problem Formulation

In recent years, FO fuzzy controllers have been extensively utilised to control dynamical systems. These controllers are designed and implemented by replacing the integer operators with fractional operators in fuzzy structures. As a demonstration, the basic integer order fuzzy PI and FO fuzzy PI controller structures are depicted in Fig. 2. The mathematical expression of the FO fuzzy PI controller is given as

$$u = K_3 \frac{d^{-\beta}}{dt^{-\beta}} \left[f \left(K_1 e(t), K_2 \frac{d^\alpha}{dt^\alpha} e(t) \right) \right] \quad (1)$$

where f is the mapping among the input and output of the fuzzy controller. The method of linear approximation suggested by Jantzen [39] is utilised to simplify the FO fuzzy PI controller as

$$u = K_3 \frac{d^{-\beta}}{dt^{-\beta}} \left(K_1 e(t) + K_2 \frac{d^\alpha}{dt^\alpha} e(t) \right) \\ u = K_1 K_3 \frac{d^{-\beta}}{dt^{-\beta}} e(t) + K_2 K_3 \frac{d^{\alpha-\beta}}{dt^{\alpha-\beta}} e(t) \quad (2)$$

The approximation reduces the complexity of the controller while retaining its properties. The Eq. (2) is directly considered FOPI control action, whereas the control action generated is not only PI, but it depends on the values of α and β . The actual control action generated by u depending on α and β is as follows

$$u = \begin{cases} \text{Fractional order } I + D \text{ action} & \text{if } \alpha > \beta \\ \text{Fractional order } I + I \text{ action} & \text{if } \alpha < \beta \\ \text{Fractional order } P + I \text{ action} & \text{if } \alpha = \beta \end{cases} \quad (3)$$

Hence, analytically the control signal u generates FO fuzzy PI action if and only if $\alpha = \beta$. It is revealed from the literature [29–37] that various authors have considered $\alpha \neq \beta$ and claimed the structure as FO fuzzy PI controller,

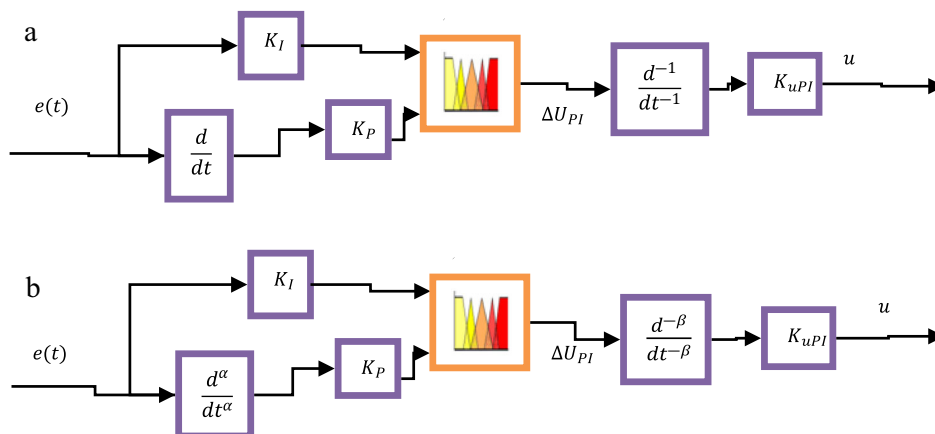


Fig. 2 Schematic block diagram of controllers **a** Fuzzy PI, and **b** FO fuzzy PI

which conflicts with mathematical formulation. This work proposes the design of the FO fuzzy PID controller based on precise mathematical derivation. The designed control structure preserves the features and properties of FOPID and the additional benefit of self-regulatory control. Also, the issues related to the stability of the fuzzy controller are addressed by deriving sufficient BIBO stability conditions for the proposed fuzzy controller. The controller performs its best with the proper tuning of its parameters. Therefore, an AI-based metaheuristic algorithm is implemented to find the design parameters of the controller according to the requirement of the system.

3 Design of FOFPI + D Controller

The derivation of FO fuzzy PI + D controller action is obtained in three stages as follows:

1. The FO fuzzy PI control action is formulated from the traditional FO PI controller.
2. The FO fuzzy D output is derived from the FO derivative action.
3. The overall action of FOFPI + D is the combination of FOFPI and FOFD controller output collectively in a suitable way, and is discussed in the next sub-sections.

3.1 Derivation of FO Fuzzy PI Control Law

The traditional FO PI control law in the Laplace domain is expressed as

$$U_{PI}(s) = \left(K_p^c + K_I^c \frac{1}{s^\lambda} \right) E(s) \tag{4}$$

where, K_p^c and K_I^c are the proportional and integral gains, respectively. $E(s)$ is the tracking error signal, and λ is the order of fractional operator. The above equation can be changed into the discrete domain by using backward transformation $s \simeq \frac{(1-z^{-1})}{T}$, Where $T > 0$ is the step time.

$$U_{PI}(z) = \left(K_p^c + K_I^c \frac{T^\lambda}{(1-z^{-1})^\lambda} \right) E(z) \tag{5}$$

$$\Delta U_{PI}(z) = \left(K_p^c (1-z^{-1})^\lambda + K_I^c T^\lambda \right) E(z) \tag{6}$$

where

$$\Delta U_{PI}(z) = U_{PI}(z)(1-z^{-1})^\lambda \tag{7}$$

Using power series expansion [40] on Eq. (6), yields

$$\Delta U_{PI}(z) = K_p^c \sum_{k=0}^{\infty} (-1)^k \binom{\lambda}{k} z^{-k} E(z) + K_I^c T^\lambda E(z) \tag{8}$$

Taking inverse Z-transform for Eq. (8), obtains

$$\Delta u_{PI}(nT) = K_I^c T^\lambda e(nT) + K_p^c \sum_{k=0}^{\infty} (-1)^k \binom{\lambda}{k} e((n-k)T) \tag{9}$$

The second term on the R.H.S. of Eq. (9) is analogous to the formulation proposed by Lubich for the FO differ-integral with order Ω for any function $g(nT)$ as [41]:

$$D^{\mp\Omega} g(nT) = T^{\pm\Omega} \sum_{k=0}^{\infty} (-1)^k \binom{\mp\Omega}{k} g((n-k)T) \tag{10}$$

Merging, Eq. (9) and Eq. (10) yields

$$\Delta u_{PI}(nT) = K_I^c T^\lambda e(nT) + K_p^c T^\lambda D^\lambda e(nT)$$

or simply

$$\Delta u_{PI}(nT) = K_I e(nT) + K_P e_r(nT) \tag{11}$$

where, $K_P = K_p^c T^\lambda$, $K_I = K_I^c T^\lambda$, $e_r(nT) = D^\lambda e(nT)$. Moreover, solving Eq. (7) for control action gives

$$U_{PI}(z) = \sum_{k=0}^{\infty} (-1)^k \binom{-\lambda}{k} \Delta U_{PI}(z) z^{-k} \tag{12}$$

$$u_{PI}(nT) = \sum_{k=0}^{\infty} (-1)^k \binom{-\lambda}{k} \Delta u_{PI}((n-k)T) \tag{13}$$

$$u_{PI}(nT) = T^{-\lambda} D^{-\lambda} (\Delta u_{PI}(nT)) \tag{14}$$

Replacing the term $T^{-\lambda}$ by gain K_{uPI} and $\Delta u_{PI}(nT)$ by FO fuzzy PI control action, such that

$$u_{PI}(nT) = K_{uPI} D^{-\lambda} (\Delta u_{PI}(nT)) \tag{15}$$

The structure of FOFPI is designed using Eq. (11) with $K_I e(nT)$ and $K_P e_r(nT)$ as inputs and $\Delta u_{PI}(nT)$ as control action of the FOFPI component. Where K_{uPI} is the scaling gain of the FOFPI control action.

3.2 Derivation of FO Fuzzy D Control Law

The conventional FO derivative control action for input as x and action as u_D is described in Eq. (16) as

$$U_D(s) = K_D^c s^\lambda X(s) \tag{16}$$

Applying the backward transformation, $s \simeq \frac{(1-z^{-1})}{T}$

$$U_D(z) = \frac{K_D^c (1-z^{-1})^\lambda X(z)}{T^\lambda} \tag{17}$$

$$\Delta U_D(z) = K_D^c \sum_{k=0}^{\infty} (-1)^k \binom{\lambda}{k} X(z) z^{-k} \tag{18}$$

where

$$\Delta U_D(z) = T^\lambda U_D(z) \tag{19}$$

Applying inverse Z- transform to Eq. (18) yields

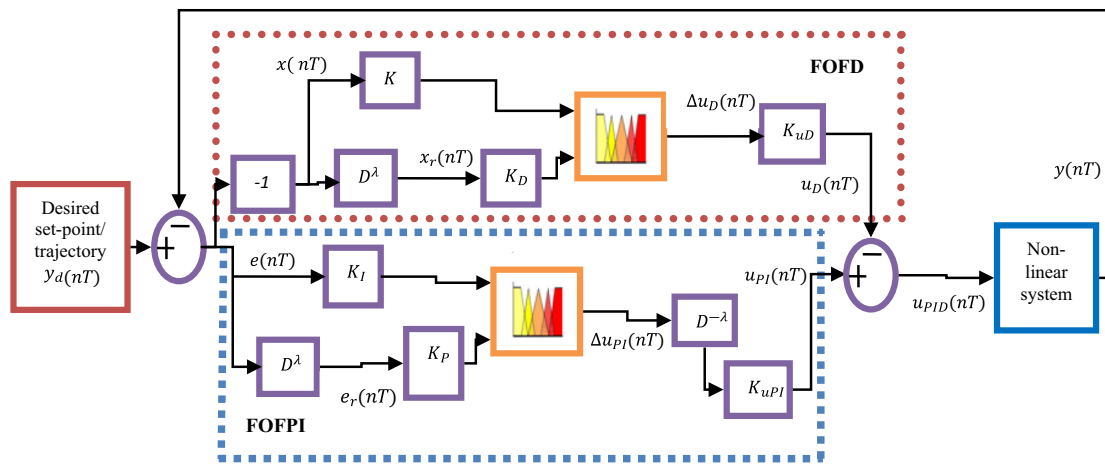


Fig. 3 Generalised control structure of FOFPI + D for dynamic system

$$\Delta u_D(nT) = K_D^c \sum_{k=0}^{\infty} (-1)^k \binom{\lambda}{k} x((n-k)T) \tag{20}$$

$$\Delta u_D(nT) = K_D^c T^\lambda D^\lambda x(nT) \tag{21}$$

$$\Delta u_D(nT) = K_D D^\lambda x(nT) \tag{22}$$

It is difficult to generate meaningful fuzzy control action depending on a single input. Therefore, the control law of Eq. (22) is modified by adding a signal $Kx(nT)$ to its right-hand side as an input of the FOFD component.

$$\Delta u_D(nT) = Kx(nT) + K_D x_r(nT) \tag{23}$$

where $K_D = K_D^c T^\lambda$, $x(nT) = -e(nT) = y(nT) - y_d(nT)$, $x_r(nT) = D^\lambda x(nT)$ and solving the Eq. (19) for control action

$$U_D(z) = T^{-\lambda} \Delta U_D(z) \tag{24}$$

$$u_D(nT) = T^{-\lambda} \Delta u_D(nT) \tag{25}$$

When $\Delta U_D(nT)$ is converted to FOFD control law, and the term $T^{-\lambda}$ is replaced by gain K_{uD} , then Eq. (25) can be rewritten as

$$u_D(nT) = K_{uD} \Delta u_D(nT) \tag{26}$$

The structure of the FOFD component is modelled by Eq. (23) with $\Delta u_D(nT)$ as control action and $Kx(nT)$ and $K_D x_r(nT)$ as inputs of the FOFD component.

3.3 Inclusive FO Fuzzy PI + D Control Law

At last, overall FOFPI + D controller action is achieved by subtracting the action of FOFD component Eq. (26) from FOFPI component Eq. (15) collectively as

$$u_{PID}(nT) = u_{PI}(nT) - u_D(nT) \tag{27}$$

Or

$$u_{PID}(nT) = K_{uPI} D^{-\lambda} (\Delta u_{PI}(nT)) - K_{uD} \Delta u_D(nT) \tag{28}$$

Based on the mathematical model described above, the generalised control structure of the FOFPI + D controller for the non-linear dynamic system is shown in Fig. 3.

3.4 Implementation of Fractional Operators

Fractional calculus has become integral to various engineering applications in the past decade. Several methods for realising fractional operators are recorded in the literature [42, 43]. This work uses a digital approximation of the fractional operator defined by Lubich [41]. The implementation in a discrete domain involves the binomial expansion of backward transformation in $s^{\pm\mu}$ as follows

$$s^{\pm\mu} = \left(\frac{1-z^{-1}}{T} \right)^{\pm\mu} \tag{29}$$

$$s^{\pm\mu} = T^{\mp\mu} \sum_{k=0}^{\infty} (-1)^k \frac{(\pm\mu)(\pm\mu-1)(\pm\mu-2)\dots(\pm\mu-k+1)}{k!} z^{-k} \tag{30}$$

Denoting discrete-time differ-integral operator as ‘D’, the designed fractional differentiator/integrator in the discrete domain is represented as

$$D^{\mp\mu} = T^{\pm\mu} \sum_{k=0}^{\infty} (-1)^k \binom{\mp\mu}{k} z^{-k} \tag{31}$$

Practical realisation of the Eq. (31) requires the calculation of the infinite number of coefficients. Hence, the short memory principle is implemented to design fractional operators as

$$D^{\mp\mu} g(nT) = T^{\pm\mu} \sum_{k=0}^M (-1)^k \binom{\mp\mu}{k} g((n-k)T) \tag{32}$$

where $g(nT)$ is an arbitrary discrete function, α is the order of operator, M is memory size, and its value is 100.

3.5 The Analytical Design of Fuzzy Control

This section presents the design of fuzzy systems using standard methodology, which includes fuzzification, creating rule base, and defuzzification procedure.

3.5.1 Fuzzification

The FOFPI and FOFD components of the FOFPI + D controller are fuzzified separately. Then, the rule base of both the components is combined by considering the FOFPI + D control law in Eq. (27). FOFPI component utilises 2 inputs: error signal $\tilde{e}(nT) = K_I e(nT)$ and fractional rate of error $\tilde{e}_r(nT) = K_P e_r(nT)$. Similarly, the FOFD component of the controller has inputs $\tilde{x}(nT) = Kx(nT)$ and $\tilde{x}_r(nT) = K_D x_r(nT)$. For each input, two triangular membership functions denoted as n : negative and p : positive are designated. FOFPI and FOFD blocks have single control output $\Delta u_{PI}(nT)$ and $\Delta u_D(nT)$ respectively, which are fuzzified using three singleton membership functions. Figure 4 portrays the membership functions for input and output of FOFPI and FOFD components, where $L > 0$ and its value is obtained through optimisation.

3.5.2 Formulation of Control Rules for FOFPI and FOFD

The rule base for the fuzzy inference system is designed based on either expert experience or control system knowledge. This work establishes four fuzzy control rules based on control system knowledge for each FOFPI and FOFD controller. Depending on membership functions, the following control rule base is framed for the FOFPI controller:

- (Cr₁) – If $\tilde{e} = \tilde{e}.n$ and $\tilde{e}_r = \tilde{e}_r.n$ then $\Delta u_{PI} = o.n$
- (Cr₂) – If $\tilde{e} = \tilde{e}.n$ and $\tilde{e}_r = \tilde{e}_r.p$ then $\Delta u_{PI} = o.z$
- (Cr₃) – If $\tilde{e} = \tilde{e}.p$ and $\tilde{e}_r = \tilde{e}_r.n$ then $\Delta u_{PI} = o.z$

- (Cr₄) – If $\tilde{e} = \tilde{e}.p$ and $\tilde{e}_r = \tilde{e}_r.p$ then $\Delta u_{PI} = o.p$

where $\tilde{e} = K_I e = K_I (y_d - y)$ is the error, $\tilde{e}_r = K_P e_r(nT) = K_P (D^\lambda y_d - D^\lambda y)$ is the fractional rate of error and Δu_{PI} is the output of the FOFPI component. ' $\tilde{e}.n$ ' signifies error negative, ' $\tilde{e}_r.p$ ' implies the fractional derivative of error is positive, and ' $o.z$ ' is output zero. Similarly, control rules for FOFD controller are framed as follows:

- (Cr₅) – If $\tilde{x} = \tilde{x}.p$ and $\tilde{x}_r = \tilde{x}_r.p$ then $\Delta u_D = o.z$
- (Cr₆) – If $\tilde{x} = \tilde{x}.p$ and $\tilde{x}_r = \tilde{x}_r.n$ then $\Delta u_D = o.p$
- (Cr₇) – If $\tilde{x} = \tilde{x}.p$ and $\tilde{x}_r = \tilde{x}_r.n$ then $\Delta u_D = o.n$
- (Cr₈) – If $\tilde{x} = \tilde{x}.n$ and $\tilde{x}_r = \tilde{x}_r.n$ then $\Delta u_D = o.z$

In these control rules: $\tilde{x} = Kx = K(y - y_d)$, $\tilde{x}_r = K_D x_r = K_D D^\lambda x$, Δu_D is the output of the FOFD component. The set of eight rules together determines the overall control law of the FOFPI + D controller. The significance of control rules is explained as.

In control rule 1 (Cr₁): condition $\tilde{e}.n$ (error negative) implies that output y of the system is above the desired output y_d , & $\tilde{e}_r.n$ (a fractional derivative of error is negative) infers $D^\lambda y > D^\lambda y_d$ (means system output is moving upwards faster than desired output). Therefore, to keep output y close to the desired signal y_d , the output of the FOFPI component Δu_{PI} is set as negative. In the case of the FOFD component, control rule 5 (Cr₅) is fired corresponding to Cr₁, and its output Δu_D is set to be zero. Thus, by Cr₁ and Cr₅ of both components, the overall control law as given in Eq. (27) drives the output of the system downwards. The system output can also be driven faster if the FOFD component output is positive. But both component outputs being non-zero simultaneously, complicates controller design.

In control rule 2 (Cr₂), the system output is above the desired output but moves downwards faster than the desired output. So, Δu_{PI} is set zero and Δu_D is made

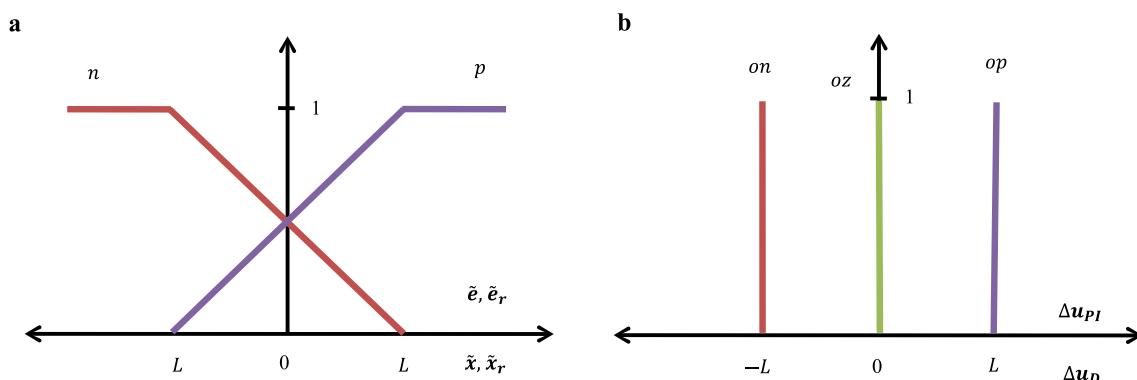


Fig. 4 Membership functions for a Inputs & b Output of FOFPI and FOFD

positive to bring the system output down by combining Cr_2 and Cr_6 . Similarly, other rules can also be explained.

3.5.3 Defuzzification

Defuzzification is converting the fuzzy value to a crisp value; several methods are available in the literature to defuzzify the fuzzy output. The selection of the defuzzification method for a specific problem is a critical and challenging task. Driankov et al. [44] evaluated and compared the performance of different defuzzification methods for control applications. The study suggested that the centroid/centre of mass defuzzification method proved more efficient than other techniques. Therefore, in this work centre of mass formula to defuzzify FOFPI and FOFD components is used [19]. The control action Δu_{PI} and Δu_D based on the defuzzification method is described as

$$\Delta u = \frac{\sum(\text{output corresponding to membership value of input} \times \text{membership value of input})}{\sum \text{membership value of input}} \tag{33}$$

e FOFPI inputs, i.e. error and fractional error rate, are divided into 20 input combination (IC) regions and are graphically depicted in Fig. 5. The horizontal axis represents the membership functions of the error $K_I e(nT)$ and that of the fractional rate of error $K_P e_r(nT)$ is represented on the vertical axis. The control rules (Cr_1 to Cr_4), membership functions, and the IC regions are used to evaluate each region's fuzzy control law of the FOFPI controller. Considering region IC1 and Cr_1 , the value of $\tilde{e}.n < 0.5$ and

$\tilde{e}_r.n > 0.5$ from Fig. 4a, therefore by using Zadeh's logic [45]

$$\tilde{e} = \tilde{e}.n \text{ and } \tilde{e}_r = \tilde{e}_r.n \text{ implies } \min\{\tilde{e}.n, \tilde{e}_r.n\} = \tilde{e}.n$$

Therefore, from Cr_1 ,

$$(Cr_1) \left\{ \begin{array}{l} \text{The chosen input membership function is } \tilde{e}.n \\ \text{The membership value of output is } o.n \end{array} \right.$$

Similarly, other rules and Zadeh's logic yields

$$(Cr_2) \left\{ \begin{array}{l} \text{The chosen input membership function is } \tilde{e}.n \\ \text{The membership value of output is } o.z \end{array} \right.$$

$$(Cr_3) \left\{ \begin{array}{l} \text{The chosen input membership function is } \tilde{e}_r.n \\ \text{The membership value of output is } o.z \end{array} \right.$$

$$(Cr_4) \left\{ \begin{array}{l} \text{The chosen input membership function is } \tilde{e}_r.p \\ \text{The membership value of output is } o.p \end{array} \right.$$

The values of $o.p = L, o.n = -L, o.z = 0$ are from Fig. 4b, and by applying the geometry of straight line to the membership functions of input, following formula are derived [27]:

$$e.p = \frac{K_I e(nT) + L}{2L}, e.n = \frac{-K_I e(nT) + L}{2L}$$

$$e_r.p = \frac{K_P e_r(nT) + L}{2L}, e_r.n = \frac{-K_P e_r(nT) + L}{2L}$$

Now, substituting the above formulae and values in Eq. (33), the output $\Delta u_{PI}(nT)$ in region IC1 is obtained as,

$$\Delta u_{PI}(nT) = \frac{L(K_I e(nT) + K_P e_r(nT))}{2(2L - K_I e(nT))}$$

Rearranging the above equation yields

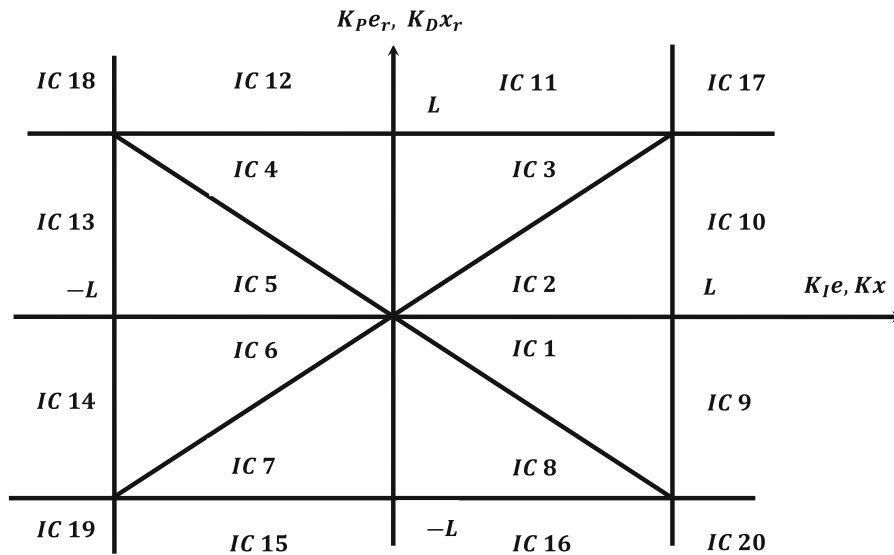


Fig. 5 Input combination region for both FOFPI and FOFD components

Table 1 Formulae for Δu_{PI} and Δu_D for all regions of IC

IC regions	FOFPI output (Δu_{PI})	FOFD output (Δu_D)
IC1, 2, 5, 6	$\frac{L(K_I e(nT) + K_P e_r(nT))}{2(2L - K_I e(nT))}$	$\frac{L(Kx(nT) - K_D x_r(nT))}{2(2L - K x(nT))}$
IC3, 4, 7, 8	$\frac{L(K_I e(nT) + K_P e_r(nT))}{2(2L - K_P e_r(nT))}$	$\frac{L(Kx(nT) - K_D x_r(nT))}{2(2L - K_D x_r(nT))}$
IC9, 10	$\frac{1}{2}(L + K_P e_r(nT))$	$\frac{1}{2}(-K_D x_r(nT) + L)$
IC11, 12	$\frac{1}{2}(L + K_I e(nT))$	$\frac{1}{2}(Kx(nT) - L)$
IC13, 14	$\frac{1}{2}(K_P e_r(nT) - L)$	$\frac{1}{2}(-K_D x_r(nT) - L)$
IC15, 16	$\frac{1}{2}(K_I e(nT) - L)$	$\frac{1}{2}(Kx(nT) + L)$
IC17	L	0
IC18	0	$-L$
IC19	$-L$	0
IC20	0	L

$$\Delta u_{PI}(nT) = \left[\frac{LK_I}{2(2L - K_I e(nT))} \right] e(nT) + \left[\frac{LK_P}{2(2L - K_I e(nT))} \right] e_r(nT) \tag{34}$$

The control law Eq. (34) follows the linearity property of classical controller with the difference that its gains vary nonlinearly as the function of input signals $e(nT)$. These non-linear gains provide adaptive/self-regulatory features to the controller. Similarly, all the control laws for FOFPI and FOFD components for each IC region are obtained and listed in Table 1. The following section establishes sufficient stability conditions for the control loop using the two straight lines method (graphical approach).

3.6 Stability Analysis Using a Graphical Approach

The sufficient stability condition for fuzzy PI/PD/PID controller has been determined using the acclaimed small gain theorem. For a BIBO stable system, the output of the system is bounded at all times in the case of bounded input. The obtained conditions by the analysis help design a safe fuzzy control and provide guaranteed closed-loop stability. The BIBO stability of FO fuzzy PI + D controller in a closed-loop is investigated analytically using a graphical approach [23, 28].

Now by considering Fig. 3, it is clear that $x(nT)$ and $x_r(nT)$ have an opposite sign as compared to $e(nT)$ and $e_r(nT)$, respectively. Thus, overall control action $u_{PID}(nT)$ of closed-loop control, the structure depends on $e(nT)$ and $e_r(nT)$. In the discrete domain, let

$$a(z) = \frac{e(z)}{u_{PID}(z)} \text{ and } b(z) = \frac{e_r(z)}{u_{PID}(z)}$$

where

$$a(z) = a_0 + a_1 z^{-1} + a_2 z^{-2} + \dots$$

$$b(z) = b_0 + b_1 z^{-1} + b_2 z^{-2} + \dots$$

Here coefficients are unknown. In the same way,

$$e(z) = e_0 + e_1 z^{-1} + e_2 z^{-2} + \dots$$

$$e_r(z) = e_{r_0} + e_{r_1} z^{-1} + e_{r_2} z^{-2} + \dots$$

$$u_{PID}(z) = u_{PID0} + u_{PID1} z^{-1} + u_{PID2} z^{-2} + \dots$$

Let

$$A = \sum_{i=0}^{\infty} |a_i|, \text{ and } B = \sum_{i=0}^{\infty} |b_i|$$

$$E = \sum_{i=0}^{\infty} |e_i|, R = \sum_{i=0}^{\infty} |e_{r_i}| \text{ and } U = \sum_{i=0}^{\infty} |u_{PIDi}|,$$

Now for the closed-loop system to be BIBO stable, both $\|A\|$ and $\|B\|$ must be finite, thus

$$\|A\| = \alpha_1$$

$$\|B\| = \alpha_2$$

where α_1 and α_2 are constants. Also, we have

$$\|E\| \leq \alpha_1 \|U\| \tag{35}$$

$$\|R\| \leq \alpha_2 \|U\| \tag{36}$$

Suppose that

$$y(nT + T) = \aleph(y(nT)) + H_1(u_{PID}(nT)) + H_2(w(nT))$$

where, \aleph is an operator of a closed-loop scheme, $w(nT)$ are corresponding disturbances in the system ($H_2 = 0$ if it does not exist), and \aleph, H_1, H_2 are bounded non-linear functions (in norm operator), such that:

$$\|\aleph\| < \infty, \|H_1\| < \infty, \|H_2\| < \infty$$

Then, it follows that

$$\|H_1(u_{PID}(nT))\| = \|y(nT + T) - \aleph(y(nT)) - H_2(w(nT))\|$$

$$\|H_1(u_{PID}(nT))\| \leq \|y(nT + T)\| + \|\aleph\| \times \|y(nT)\| + \|H_2\| \times \|w(nT)\|$$

Also, $\|H_1(u_{PID}(nT))\| \leq \|H_1\| \times \|(u_{PID}(nT))\|$ to assure that LHS be bounded, then

$$\|H_1\| \times \|(u_{PID}(nT))\| \leq \|y(nT + T)\| + \|\aleph\| \times \|y(nT)\| + \|H_2\| \times \|w(nT)\|$$

Or, still more conventionally as

$$\|(u_{PID}(nT))\| \leq \beta_1 + \beta_2 \|E\| + \beta_3 \|R\| \tag{37}$$

where

$$\beta_1 \leq \frac{1}{\|H_1\|} (\|y(nT + T)\| + \|\aleph\| \times \|y(nT)\| + \|H_2\| \times \|w(nT)\|)$$

$$\beta_2 \leq \max\{\|K_I\|, \|K\|\}$$

$$\beta_3 \leq \max\{\|K_P\|, \|K_D\|\}$$

Substituting, Eq. (37) in Eqs. (35) and (36) yields

$$\|E\| \leq \alpha_1(\beta_1 + \beta_2\|E\| + \beta_3\|R\|)$$

Explicitly,

$$\|R\| \geq \frac{1}{\alpha_1\beta_3}[(1 - \alpha_1\beta_2)\|E\| - \alpha_1\beta_1] \quad (38)$$

and

$$\|R\| \leq \frac{1}{1 - \alpha_2\beta_3}[\alpha_2\beta_2\|E\| + \alpha_2\beta_1] \quad (39)$$

Comparing the above Eqs. (38) and (39) with the general equation of the straight line (i.e. $\|R\| = \text{slope} * \|E\| + \text{constant}$) in $\|E\|-\|R\|$ the plane provides information about the slope and constant. The sufficient condition for the closed-loop system to be stable is achieved by examining the four cases as. **Case 1.** When $\alpha_1\beta_2 > 1$ and $\alpha_2\beta_3 < 1$:

Under this condition, the slope of Eq. (38) is negative, and Eq. (39) is positive. The intersection region produced by plotting both the lines is shown in Fig. 6a. In this case, there exists an unbounded region in the first quadrant of $\|E\|-\|R\|$ plane. Thus, the closed-loop system is unbounded; and the case is avoided.

Case 2. When $\alpha_1\beta_2 > 1$ and $\alpha_2\beta_3 > 1$

In this condition, the slope and constant of both the straight lines are negative; therefore, no bounded region exists in the first quadrant of $\|E\|-\|R\|$ plane, as shown in Fig. 6b. Therefore, this case does not provide the condition of stability and should be abolished.

Case 3. When $\alpha_1\beta_2 < 1$ and $\alpha_2\beta_3 > 1$

The slope and constant of Eq. (38) are positive and negative, respectively, and for Eq. (39) both are negative. In this situation, there is an empty region in the first quadrant, as shown in Fig. 6c. Therefore this case is also discarded.

Case 4. When $\alpha_1\beta_2 < 1$ and $\alpha_2\beta_3 < 1$

In this case slope of both lines are positive, with constants having the opposite sign. Therefore, the lines intersect in the first quadrant with a common region, as shown in Fig. 6d. The common region is bounded within the first quadrant of $\|E\|-\|R\|$ plane. Thus, a sufficient stability condition exists and is derived by equating the Eqs. (38) and (39).

$$\begin{aligned} & \frac{1}{\alpha_1\beta_3}[(1 - \alpha_1\beta_2)\|E_Q\| - \alpha_1\beta_1] \\ &= \frac{1}{1 - \alpha_2\beta_3}[\alpha_2\beta_2\|E_Q\| + \alpha_2\beta_1], \end{aligned}$$

where $\|E_Q\|$ is the value of $\|E\|$ at the point of intersection of two lines. Solving for $\|E_Q\|$ gives

$$E_Q = \frac{\alpha_1\beta_1}{1 - (\alpha_1\beta_2 + \alpha_2\beta_3)}$$

Similarly, $\|R_Q\|$ is obtained as

$$\|R_Q\| = \frac{\alpha_2\beta_1}{1 - (\alpha_1\beta_2 + \alpha_2\beta_3)}$$

Hence, the lines intersect at a point,

$$(\|E_Q\|, \|R_Q\|) = \left(\frac{\alpha_1\beta_1}{1 - (\alpha_1\beta_2 + \alpha_2\beta_3)}, \frac{\alpha_2\beta_1}{1 - (\alpha_1\beta_2 + \alpha_2\beta_3)} \right)$$

The coordinate of the point is finite and bounded; when $\alpha_1\beta_2 + \alpha_2\beta_3 < 1$.

Lemma 1 The sufficient condition of stability for FOFPI + D in the control loop are summarised as

- $\|E\| \leq \alpha_1\|U\|, \|R\| \leq \alpha_2\|U\|$
- $\alpha_1\beta_2 + \alpha_2\beta_3 < 1$
- $\beta_1 \leq \frac{1}{\|H_1\|}(\|y(nT + T)\| + \|\mathfrak{N}\| \times \|y(nT)\| + \|H_2\| \times \|w(nT)\|)$
- $\beta_2 \leq \max\{\|K_I\|, \|K\|\}$
- $\beta_3 \leq \max\{\|K_P\|, \|K_D\|\}$
- $\alpha_1\beta_2 < 1, \alpha_2\beta_3 < 1$

Finally, the norm $\|y\|$ in statement c) of lemma1 needs not to be finite when validating term β_1 , if $\|y\| = \infty$ at that moment, statement c) is trivially fulfilled. Nevertheless, if all the remaining statements are satisfied concurrently, then $\|y\|$ undoubtedly will be finite as an outcome of the stability of closed-loop configuration.

3.7 Multiobjective Optimisation and NSGA-II

The proposed FOFPI + D controller has additional design parameters associated with fuzzy logic and fractional order operators, thereby increasing the computational complexity. The design of the controller requires a large amount of calculation and the controller performs its best with fine tuning only. There are different methods to find the controller parameters; nevertheless, with the advancement in artificial intelligence, the optimum parameters can be found easily using AI-based metaheuristics algorithms. In this work, an efficient multiobjective evolutionary optimisation algorithm is utilised to deal with the large computations required for tuning the controller. The main goal of evolutionary algorithms is to find the optimum result by minimising the objective through the survival of the fittest criterion. The system considered in this work has conflicting objectives, and optimisation by a single objective genetic algorithm (GA) can compromise the performance. Also, these optimisation algorithms generate the final best solution to a problem, so there is no chance of obtaining a trade-off among divergent objectives. On the other hand,

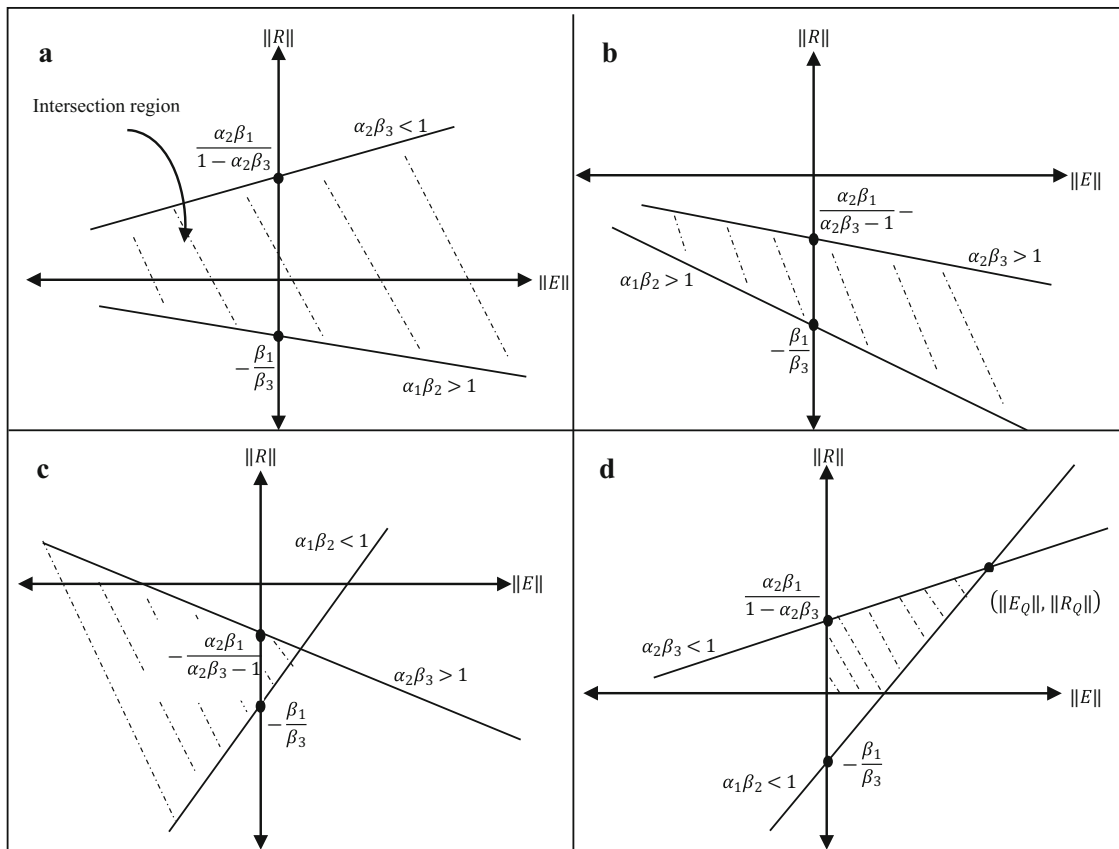


Fig. 6 Intersection region of two straight lines in $\|E\|$ - $\|R\|$ plane **a** Case 1 **b** Case 2 **c** Case 3 **d** Case 4

multiobjective optimisation minimises several objectives simultaneously besides satisfying (optional) constraints. A vector of conflicting objectives for optimisation is expressed as

$$F(\zeta) = \{f_1(\zeta), f_2(\zeta), \dots, f_m(\zeta)\}$$

Subject to:

$$q_j(\zeta) = 0 \forall j \in [1, v]$$

$$c_j \leq h_j(\zeta) \leq d_j \forall j \in [1, s],$$

where c_j and d_j are constants, ζ is the number of variables in the problem, $\zeta \in \gamma$, with γ being decision space, and R^n is objective space, also $F : \gamma \rightarrow R^n$ contains m objective functions. $h_j(\cdot)$ and $q_j(\cdot)$ are optional s inequality and v equality constraints on the problem, respectively. The objectives $f_1(\zeta), f_2(\zeta), \dots, f_m(\zeta)$ are usually conflicting. Therefore, the principle of Pareto optimality is used for simultaneous optimisation of objectives, providing acceptable solutions with the trade-off between various objectives [46].

Non-dominated sorting genetic algorithm-II (NSGA-II) is a vastly utilised multiobjective optimisation algorithm inspired by biological evolution. The supremacy of NSGA-II lies in converting multiple objectives into a single

measure by generating a set of Pareto fronts, sorted on the basis of non-domination. To solve multiple objectives problems in engineering fields, NSGA-II is implemented because of its efficiency, simplicity, and elitism [9, 10, 13, 47, 48]. NSGA-II performs all the computations in this work and finds the controller parameters for its optimum performance. The design steps for implementing NSGA-II are given in [38]. In subsequent sections, the performance of the NSGA-II optimised FOFPI + D and FPI + D controllers is evaluated for control of a non-linear robotic system.

4 Results and discussion

The performance of the proposed controllers is critically inspected for position control of the two-link robotic manipulator. This system exhibits highly non-linear characteristics and is a benchmark problem for testing the efficacy of new control designs. Therefore, the non-linear dynamics of the two-link robotic arm is simulated in a closed-loop configuration with FOFPI + D and FPI + D controllers. The control signal generated by the designed controllers provides the required torque for the angular

movement of the links. Simulations are performed in MATLAB using a fourth-order Runge–Kutta differential equation solver with a sampling time of $T = 1$ ms. The dynamics of the two-link robotic manipulator under consideration is described [49] as

$$\begin{aligned} \tau_1 = & m_2 l_2^2 \left(\ddot{\theta}_1 + \ddot{\theta}_2 \right) + (m_1 + m_2) l_1^2 \ddot{\theta}_1 + m_2 l_1 l_2 c_2 \left(2 \ddot{\theta}_1 + \ddot{\theta}_2 \right) \\ & - m_2 l_1 l_2 s_2 \dot{\theta}_1^2 - 2 m_2 l_1 l_2 s_2 \dot{\theta}_1 \dot{\theta}_2 + (m_1 + m_2) l_1 g c_1 \\ & + m_2 l_2 g c_{12} \end{aligned}$$

$$\begin{aligned} \tau_2 = & m_2 l_1 l_2 c_2 \ddot{\theta}_1 + m_2 l_1 g c_{12} + m_2 l_2^2 \left(\ddot{\theta}_1 + \ddot{\theta}_2 \right) \\ & + m_2 l_1 l_2 s_2 \dot{\theta}_1^2, \end{aligned}$$

where $c_1 = \cos\theta_1, c_2 = \cos\theta_2, c_{12} = \cos(\theta_1 + \theta_2), s_1 = \sin\theta_1$ and $s_2 = \sin\theta_2$. Subscripts 1 and 2 represent the parameters of link1 and link2, respectively. The angular position of link1 (θ_1) is measured w.r.t X-axis of the reference frame, whereas angular position (θ_2) for link2 is measured w.r.t link1. The torque τ_1 and τ_2 are applied at the base (starting point) of link1 and link2, respectively. The corresponding structure of the robot is depicted in Fig. 7. The value of the associated parameters of the robotic manipulator is recorded in Table 2.

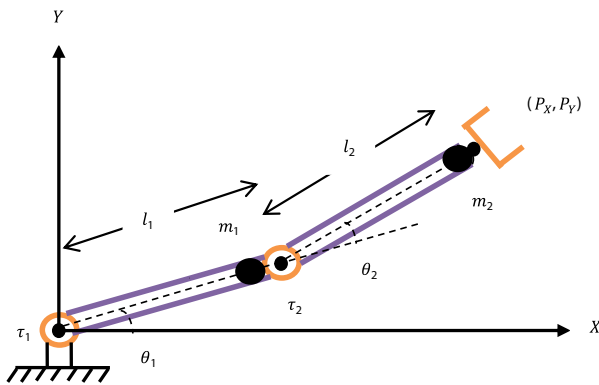


Fig. 7 Structure of the two-link robot

Table 2 Description and value of parameters for robotic manipulator [50]

Description	Symbols	Nominal value	SI units
Mass of link1	m_1	0.1	Kg
Mass of link2	m_2	0.1	Kg
Length of link1	l_1	0.8	M
Length of link2	l_2	0.4	M
Gravity constant	g	9.81	m/s^2
The angular position of link1 and link2	θ_1 and θ_2	–	Rad
Torques applied to joints of link1 and link2	τ_1 and τ_2	–	Nm

The closed-loop configuration for position control of the robotic manipulator with the FOFPI + D controller is shown in Fig. 8. Constraints applied on τ_1 and τ_2 for controlling the angular position of links are taken as $[-5, 5]$ Nm to avoid the manipulator wear and tear. The designed controllers are tested for trajectory tracking with and without varying boundary conditions, model parametric uncertainties, and disturbance rejection.

4.1 Trajectory Tracking Performance

Generally, to perform any task, the links of the manipulator should track a predefined desired trajectory. In this regard, the desired trajectory is considered as a cubic polynomial of time 't' as [50]:

$$\theta_{d_i}(t) = a_{0i} + a_{1i}t + a_{2i}t^2 + a_{3i}t^3$$

Satisfying the boundary condition

$$\left[\theta_{d_i}(t) \Big|_{t=2s}, \dot{\theta}_{d_i}(t) \Big|_{t=2s}, \theta_{d_i}(t) \Big|_{t=4s}, \dot{\theta}_{d_i}(t) \Big|_{t=4s} \right],$$

where $i = 1, 2$ specifies link1 and link2, respectively, θ_{d_i} is desired position and $\dot{\theta}_{d_i}$ is the corresponding velocity. Initial boundary condition for desired trajectory is chosen as $[1, 0, 0.5, 0]$ for link1 and $[2, 0, 4, 0]$ for link2. The search space for the controller parameter is restricted to $[0, 200]$ for K_I & K_D ; $[0, 50]$ for L_i, K_{P_i} & K_{D_i} ; $[0, 500]$ for K_{uPI_i} & K_{uD_i} and $[0, 1]$ for fractional operator λ_i .

The controller parameters are optimised using multiobjective NSGA-II with maximum iterations of 100. The problem for optimisation is formulated by defining objectives regarding absolute position error and torque variations for the two-link robotic manipulator. Their mathematical formulation is given in Eqs. (40) and (41). These objectives are contrary and conflicting (i.e., reducing objective results in increasing the other). The multiobjective optimisation offers promising solutions by trading off these objectives.

$$f_1 = \sum |\theta_{d_1}(nT) - \theta_1(nT)| + |\theta_{d_2}(nT) - \theta_2(nT)| \quad (40)$$

$$f_2 = \sum |\tau_1(nT + T) - \tau_1(nT)| + |\tau_2(nT + T) - \tau_2(nT)| \quad (41)$$

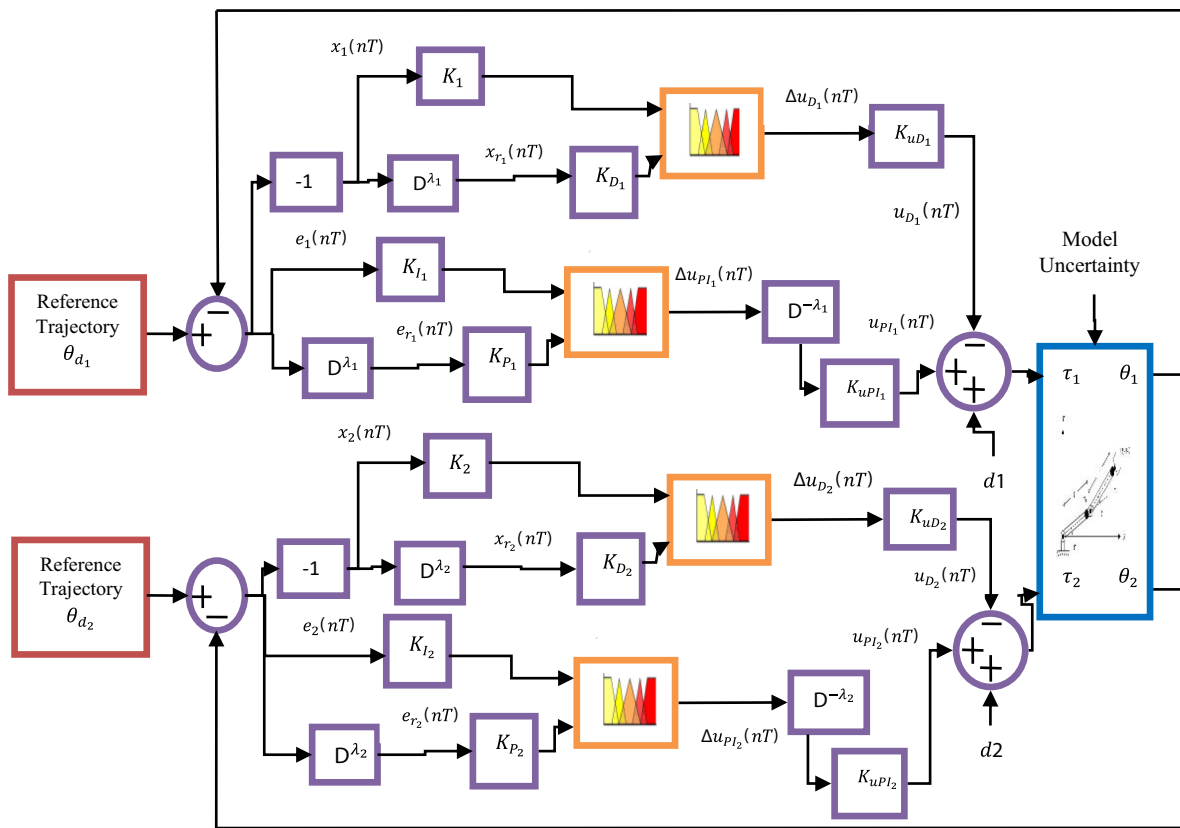


Fig. 8 Schematic block diagram of FOFPI + D controller for robotic manipulator

The time elapsed in optimising FOFPI + D is 10981.4 s, whereas for FPI + D, it is 9380.1 s. Fractional order operators are additional design variables that need tuning in the FOFPI + D controller, thus needing more time than the FPI + D controller. It makes the optimisation process more computationally complex, but it does not affect the time to generate the control signal. The control signal generation from both the controllers is unaffected by the complexity of the controllers. Figure 9 shows the Pareto front obtained for optimising the FOFPI + D and FPI + D controllers for the defined objectives. Associated optimised parameters values, objectives, and integral absolute error (IAE) for both the controllers are given in Table 3. These parameters of both controllers were kept unchanged throughout the entire simulation study.

The trajectory tracking performance of the controllers is shown in Fig. 10a, and their corresponding variations in torque, error, and end effector position in XY- plane with time are shown in Fig. 10b, c, and d, respectively. The IAE values of link1 and link2 in the FOFPI + D controller are almost 1/3 and 1/17 times that of the FPI + D controller, respectively. The improvement in IAE value is because the introduction of fractional operators in the FPI + D

controller adds extra design variables. Moreover, gains of controllers vary nonlinearly, thereby providing automated control action to the system. Thus FOFPI + D offers tight trajectory tracking over the FPI + D controller.

Further, the effectiveness of the incorporated AI technique in the proposed controllers is analysed by comparing its performance with other non-AI controllers. Various controllers such as primary PID, fractional order PID (FO-PID), non-linear PID (NL-PID), and non-linear fractional order PID (NLF-PID) are designed in the literature [11] for the control of two-link robotic manipulator with identical parameters. These controllers are also optimised by NSGA-II, making the evaluation fair. Table 4 shows the comparison of the performance of controllers in trajectory tracking based on IAE value. It can be seen from the table that the controller that has AI incorporated through fuzzy logic performs better as compared to other controllers. Later, in the subsequent section, the robustness of the controller is tested for varying boundary conditions of trajectory, model parametric uncertainties, and disturbance rejection with and without uncertainties.

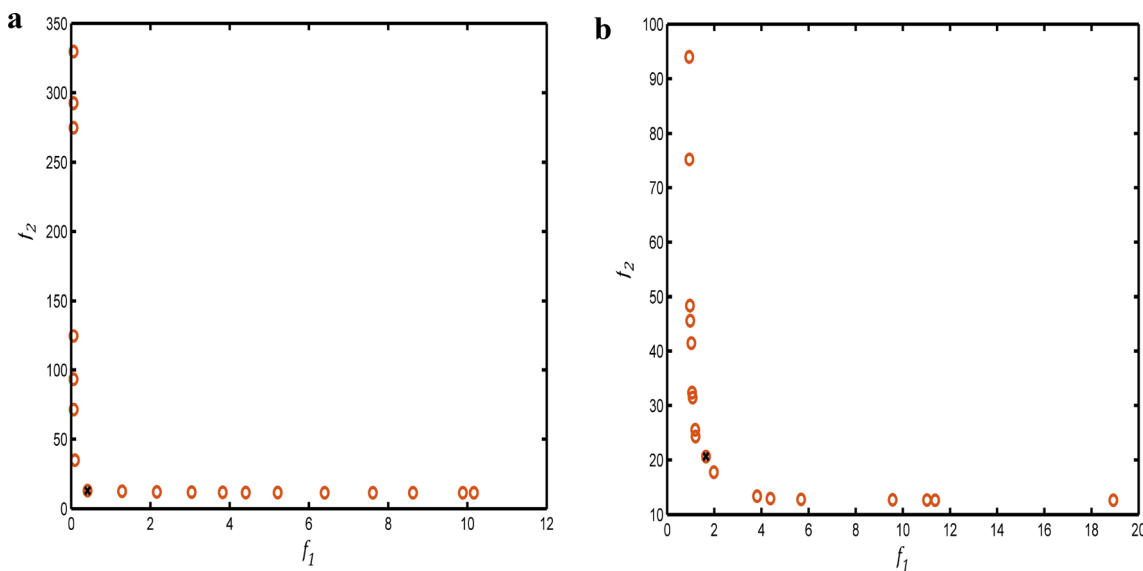


Fig. 9 Trade-off between objectives f_1 and f_2 a FOFPI + D b FPI + D with selected solution dotted black colour

Table 3 Optimum parameters of controllers for link1 and link2

Controller Parameter of link1	FOFPD + I	FPD + I	Controller Parameter of link2	FOFPD + I	FPD + I
K_{I_1}	9.844	99.8735	K_{I_2}	173.4280	101.712
K_{P_1}	25.2689	44.9371	K_{P_2}	20.701	32.8855
K_1	34.0299	76.5837	K_2	121.098	61.3959
K_{D_1}	28.5094	4.8508	K_{D_2}	33.0256	3.3378
K_{uPI_1}	8.4238	234.321	K_{uPI_2}	346.008	192.924
K_{uD_1}	282.122	24.0467	K_{uD_2}	446.571	7.0134
λ_1	0.0364	1	λ_2	0.197	1
L_1	0.1697	38.9514	L_2	3.1995	39.8923
IAE	3.799×10^{-4}	10.61×10^{-4}	IAE	3.45×10^{-5}	58.18×10^{-5}
z_1	0.4126	1.6431			
z_2	12.9924	20.6498			

Significance of bold indicates the smaller value of IAE

4.2 Trajectory Tracking for Varying Boundary Conditions

In actual situations, the robot end effector follows different trajectories in the workspace to perform various tasks. Variations in the trajectory are modelled by simultaneously varying the boundary conditions of link1, link2, and both links. The performance of control techniques is assessed based on IAE for all cases. The trajectory tracking performance and the corresponding variations in torque, position error, and position in XY-plane with time for boundary condition of $[-2, 1, 3, 2]$ and $[2, -1, -3, 1]$ for link1 and link2, respectively, are shown in Fig. 11. IAE values of both the controllers for varying boundary conditions of reference trajectory of link1, link2, and both

links simultaneously are listed in Table 5. The results show that IAE in link position by FOFPI + D is lesser than the FPI + D controller for all boundary conditions. Better performance of FOFPI + D is achieved due to the FO operator, which provides an additional parameter to the controller. Thus FOFPI + D is more robust for changes in the desired trajectory than the FPI + D controller

4.3 Model Uncertainty

The physical systems are extraordinarily complex and ill-defined, so it is pretty tedious to determine their mathematical model. Such systems always have model uncertainties. Therefore the handling of uncertainties becomes a critical issue for any controller. Including parametric

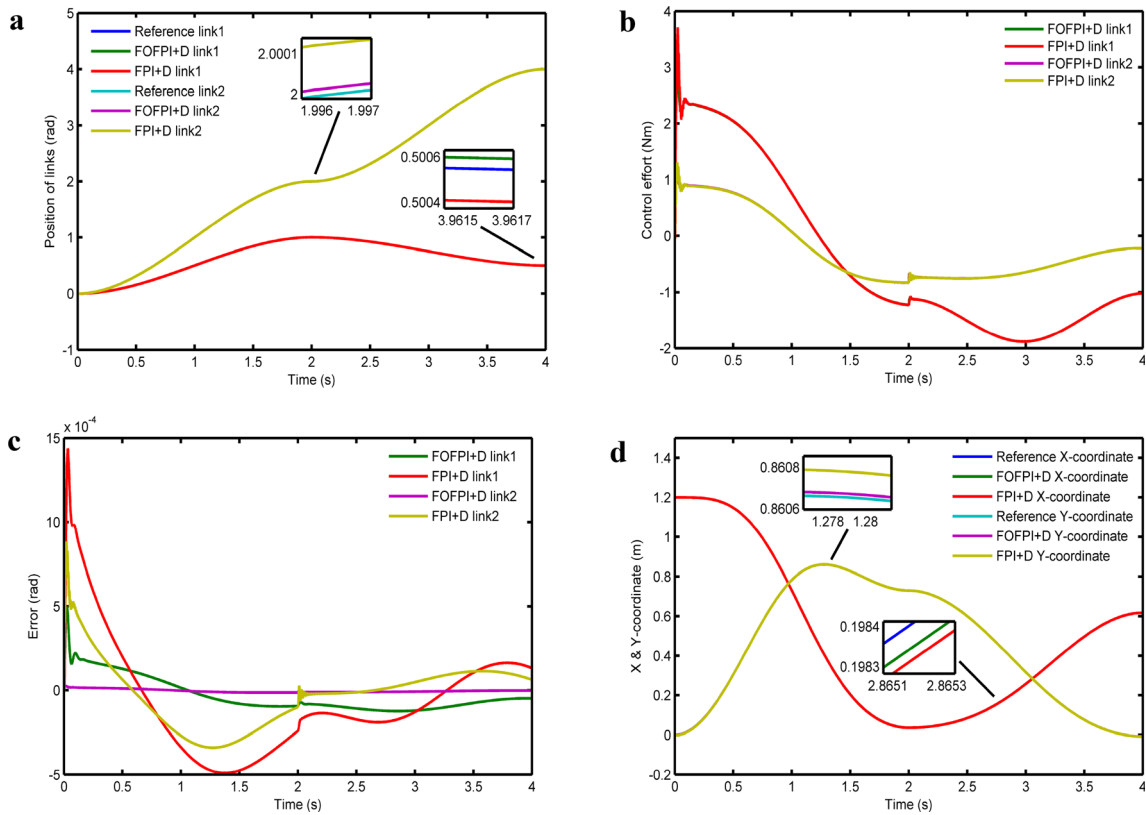


Fig. 10 Tracking response of the system with FOFPI + D and FPI + D controller **a** Links position **b** Control effort **c** Error and **d** End effector position in XY- plane

Table 4 Tracking response of the system for link1 and link2 by different controllers

Controllers	IAE in Link1	IAE in Link2
FOFPD + I	0.0003779	0.0000345
FPD + I	0.001061	0.0005818
NLF-PID	0.007508	0.002234
NL-PID	0.01269	0.004134
FO-PID	0.01841	0.008507
PID	0.02816	0.1155

uncertainties, the model of the robotic manipulator is described as:

$$\begin{aligned} \tau_1 = & (m_2 + \delta m_2)(l_2 + \delta l_2)^2 (\ddot{\theta}_1 + \ddot{\theta}_2) \\ & + (m_1 + m_2 + \delta m_1 + \delta m_2)(l_1 + \delta l_1)^2 \ddot{\theta}_1 \\ & + (m_2 + \delta m_2)(l_1 + \delta l_1)(l_2 + \delta l_2)c_2 (2\ddot{\theta}_1 + \ddot{\theta}_2) \\ & - (m_2 + \delta m_2)(l_1 + \delta l_1)(l_2 + \delta l_2)s_2 \dot{\theta}_2^2 \\ & - 2(m_2 + \delta m_2)(l_1 + \delta l_1)(l_2 + \delta l_2)s_2 \dot{\theta}_1 \dot{\theta}_2 \\ & + (m_1 + m_2 + \delta m_1 + \delta m_2)(l_1 + \delta l_1)gc_1 \\ & + (m_2 + \delta m_2)(l_2 + \delta l_2)gc_{12} \end{aligned}$$

$$\begin{aligned} \tau_2 = & (m_2 + \delta m_2)(l_1 + \delta l_1)(l_2 + \delta l_2)c_2 \ddot{\theta}_1 \\ & + (m_2 + \delta m_2)(l_1 + \delta l_1)gc_{12} \\ & + (m_2 + \delta m_2)(l_2 + \delta l_2)^2 (\ddot{\theta}_1 + \ddot{\theta}_2) \\ & + (m_2 + \delta m_2)(l_1 + \delta l_1)(l_2 + \delta l_2)s_2 \dot{\theta}_1^2, \end{aligned}$$

where

$$|\delta m_1| \leq \frac{b}{100} \times m_1, |\delta m_2| \leq \frac{b}{100} \times m_2$$

$$|\delta l_1| \leq \frac{b}{100} \times l_1, |\delta l_2| \leq \frac{b}{100} \times l_2$$

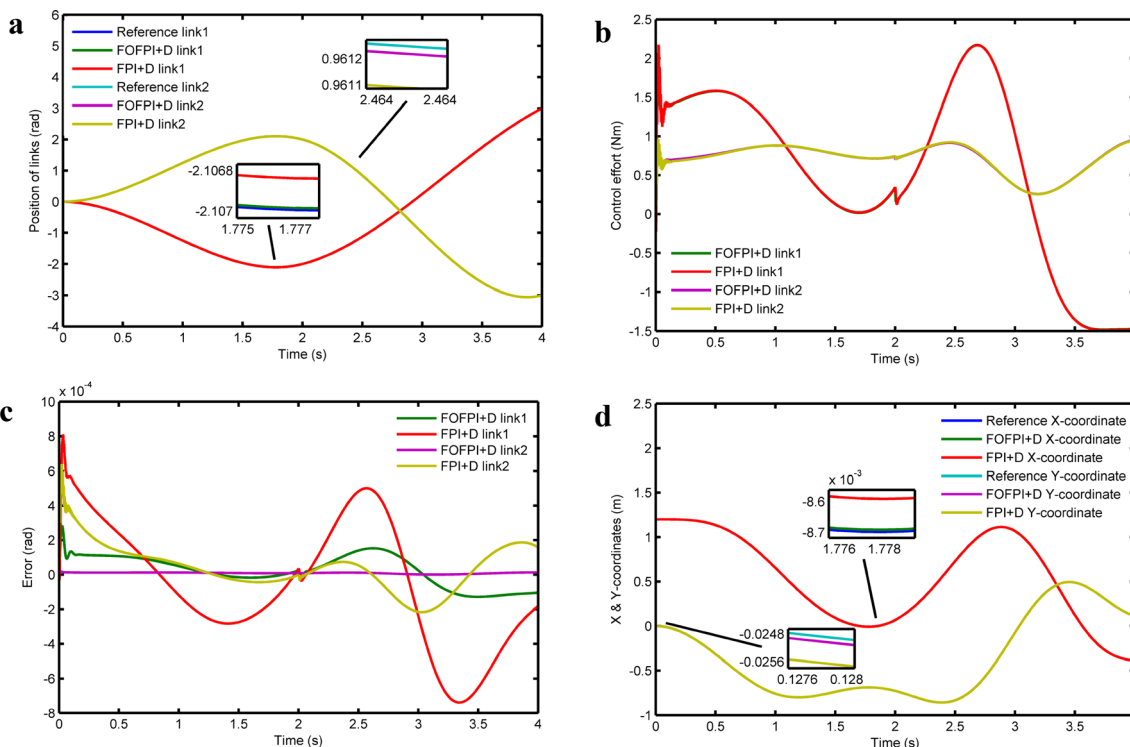


Fig. 11 Tracking response of the system with FOFPI + D and FPI + D controller **a** Links position **b** Control effort **c** Error and **d** XY-plane movement of the end effector with time for boundary condition of $[-2, 1, 3, 2]$ and $[2, -1, -3, 1]$ for link1 and link2, respectively

Table 5 IAE values for varying boundary conditions of the desired trajectory of link1, link2, and both links

Changing the boundary condition of the desired trajectory		IAE by FOFPI + D		IAE by FPI + D	
θ_{d1}	θ_{d2}	Link1 (θ_1)	Link2 (θ_2)	Link1 (θ_1)	Link2 (θ_2)
a). For link1					
$[-2, 1, 3, 2]$	$[2, 0, 4, 0]$	2.89×10^{-4}	3.96×10^{-5}	9.31×10^{-4}	68.08×10^{-5}
$[3, -2, -4, -1]$	$[2, 0, 4, 0]$	3.69×10^{-4}	2.86×10^{-5}	12.9×10^{-4}	84.42×10^{-5}
$[1, 2, 5, -3]$	$[2, 0, 4, 0]$	3.94×10^{-4}	3.92×10^{-5}	10.37×10^{-4}	98.57×10^{-5}
$[-4, -1, -7, -3]$	$[2, 0, 4, 0]$	3.33×10^{-4}	3.15×10^{-5}	7.93×10^{-4}	50.41×10^{-5}
b). For link2					
$[1, 0, 0.5, 0]$	$[2, -1, -3, 1]$	4.03×10^{-4}	3.87×10^{-5}	17.4×10^{-4}	97.27×10^{-5}
$[1, 0, 0.5, 0]$	$[-2, 2, 4, -2]$	3.63×10^{-4}	3.02×10^{-5}	15.5×10^{-4}	67.01×10^{-5}
$[1, 0, 0.5, 0]$	$[2, -1, 6, 2]$	3.95×10^{-4}	3.95×10^{-5}	14.43×10^{-4}	78.72×10^{-5}
$[1, 0, 0.5, 0]$	$[3, 1, 5, 3]$	4.1×10^{-4}	2.98×10^{-5}	12.26×10^{-4}	64.44×10^{-5}
c). For both links					
$[-2, 1, 3, 2]$	$[2, -1, -3, 1]$	3.1×10^{-4}	3.72×10^{-5}	12.25×10^{-4}	42.19×10^{-5}
$[3, -2, -4, -1]$	$[-2, 2, 4, -2]$	3.56×10^{-4}	2.77×10^{-5}	16.77×10^{-4}	55.58×10^{-5}
$[1, 2, 5, -3]$	$[2, -1, 6, 2]$	2.96×10^{-4}	3.84×10^{-5}	10.04×10^{-4}	97.23×10^{-5}
$[-4, -1, -7, -3]$	$[3, 1, 5, 3]$	3.12×10^{-4}	2.77×10^{-5}	8.24×10^{-4}	47.53×10^{-5}

Table 6 IAE in link position for $b\%$ uncertainty in parameters $m_1, m_2, l_1 \& l_2$

$b\%$ Uncertainty in $m_1, m_2, l_1 \& l_2$	IAE by FOFPI + D		IAE by FPI + D	
	Link1 (θ_1)	Link2 (θ_2)	Link1 (θ_1)	Link2 (θ_2)
± 5	3.77×10^{-4}	3.45×10^{-5}	10.53×10^{-4}	58.68×10^{-5}
± 10	3.72×10^{-4}	3.55×10^{-5}	10.36×10^{-4}	59.94×10^{-5}
± 15	3.65×10^{-4}	4.02×10^{-5}	10.13×10^{-4}	61.25×10^{-5}
± 20	3.56×10^{-4}	5.01×10^{-5}	9.82×10^{-4}	62.91×10^{-5}
± 25	3.47×10^{-4}	7.20×10^{-5}	9.46×10^{-4}	69.75×10^{-5}
± 30	3.37×10^{-4}	11.04×10^{-5}	11.39×10^{-4}	196.8×10^{-5}
± 35	3.39×10^{-4}	16.33×10^{-5}	11.71×10^{-4}	170.9×10^{-5}

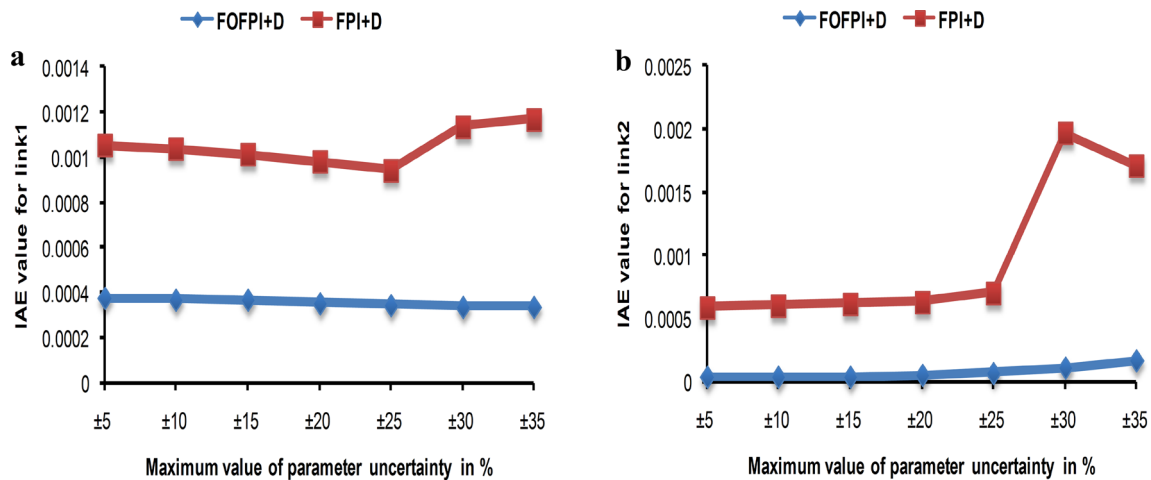


Fig. 12 Variation of IAE in link position with varying uncertainty for **a** link1 and **b** link2

b is uncertainty in mass and length of links of the system. The uncertainties ' b ' of $\pm 5\%$ to $\pm 35\%$ are introduced in the mass and length of link1 and link2, from their nominal values.

The designed FOFPI + D and FPI + D controllers are then employed to control the movement of the links. The performance of both the controllers in dealing with the uncertainty is compared on the basis of IAE in the angular position of the links. Table 6 records IAE values in the position of link1 and link2 for FOFPI + D and FPI + D controller, and a graphical depiction is represented in Fig. 12. The potentially robust FOFPI + D controller has an almost no or minor change in IAE value for every case of uncertainty in parameters. It is also evident from Fig. 12 that IAE in the position of links is relatively lower by FOFPI + D controller than FPI + D controller. The fuzzy inference technique in the FOFPI + D controller resembles human decision-making expertise. It provides the designed controller with a solid framework to handle imprecise system information and uncertainty. The control action

generated by FLC is not dependent on system dynamics, thus effectively handling the uncertainty by its reasoning. It is found from the outcomes that IAE for FOFPI + D controller is intact and lesser than its integer order counterpart for all the situations of uncertainty.

4.4 Disturbance Rejection

The unexpected disturbances generated internally or externally in practical systems are critical issues because they can deviate system output from their actual value. Thus, there is a requirement for an efficient controller which can discard such disturbances, so that response of the system accurately tracks the desired output. Therefore, disturbance rejection plays a vital role in testing the robustness of the designed controllers. Two separate studies for the disturbance rejection are performed to examine the controller's robustness. In the first study, disturbance rejection with the nominal values of system parameters is tested, and disturbance rejection with uncertain system parameters is tested in the second study.

Table 7 IAE in link position by FOFPI + D and FPI + D controller for added disturbance

Applied disturbance (Nm) in	IAE by FOFPI + D		IAE by FPI + D	
	Link1 (θ_1)	Link2 (θ_2)	Link1 (θ_1)	Link2 (θ_1)
a).d1				
2Sin50t	10.91×10^{-4}	3.45×10^{-5}	27.33×10^{-4}	59×10^{-5}
4Sin50t	20.4×10^{-4}	3.46×10^{-5}	52.32×10^{-4}	61.37×10^{-5}
6Sin50t	29.12×10^{-4}	3.47×10^{-5}	78.03×10^{-4}	65.11×10^{-5}
8Sin50t	37.08×10^{-4}	3.48×10^{-5}	104×10^{-4}	69.99×10^{-5}
10Sin50t	44.35×10^{-4}	3.49×10^{-5}	130.5×10^{-4}	76.37×10^{-5}
b).d2				
2Sin50t	3.78×10^{-4}	13.96×10^{-5}	10.66×10^{-4}	388.1×10^{-5}
4Sin50t	3.78×10^{-4}	27.61×10^{-5}	10.79×10^{-4}	772.7×10^{-5}
6Sin50t	3.78×10^{-4}	41.33×10^{-5}	11.01×10^{-4}	1160×10^{-5}
8Sin50t	3.78×10^{-4}	55.05×10^{-5}	11.31×10^{-4}	1550×10^{-5}
10Sin50t	3.78×10^{-4}	68.75×10^{-5}	11.69×10^{-4}	1945×10^{-5}
c). Both d1&d2				
2Sin50t	10.92×10^{-4}	14.03×10^{-5}	27.81×10^{-4}	392.9×10^{-5}
4Sin50t	20.41×10^{-4}	27.76×10^{-5}	53.49×10^{-4}	782.3×10^{-5}
6Sin50t	29.14×10^{-4}	41.53×10^{-5}	79.82×10^{-4}	1175×10^{-5}
8Sin50t	37.1×10^{-4}	55.29×10^{-5}	107.2×10^{-4}	1570×10^{-5}
10Sin50t	44.37×10^{-4}	69.04×10^{-5}	160.7×10^{-4}	1960×10^{-5}

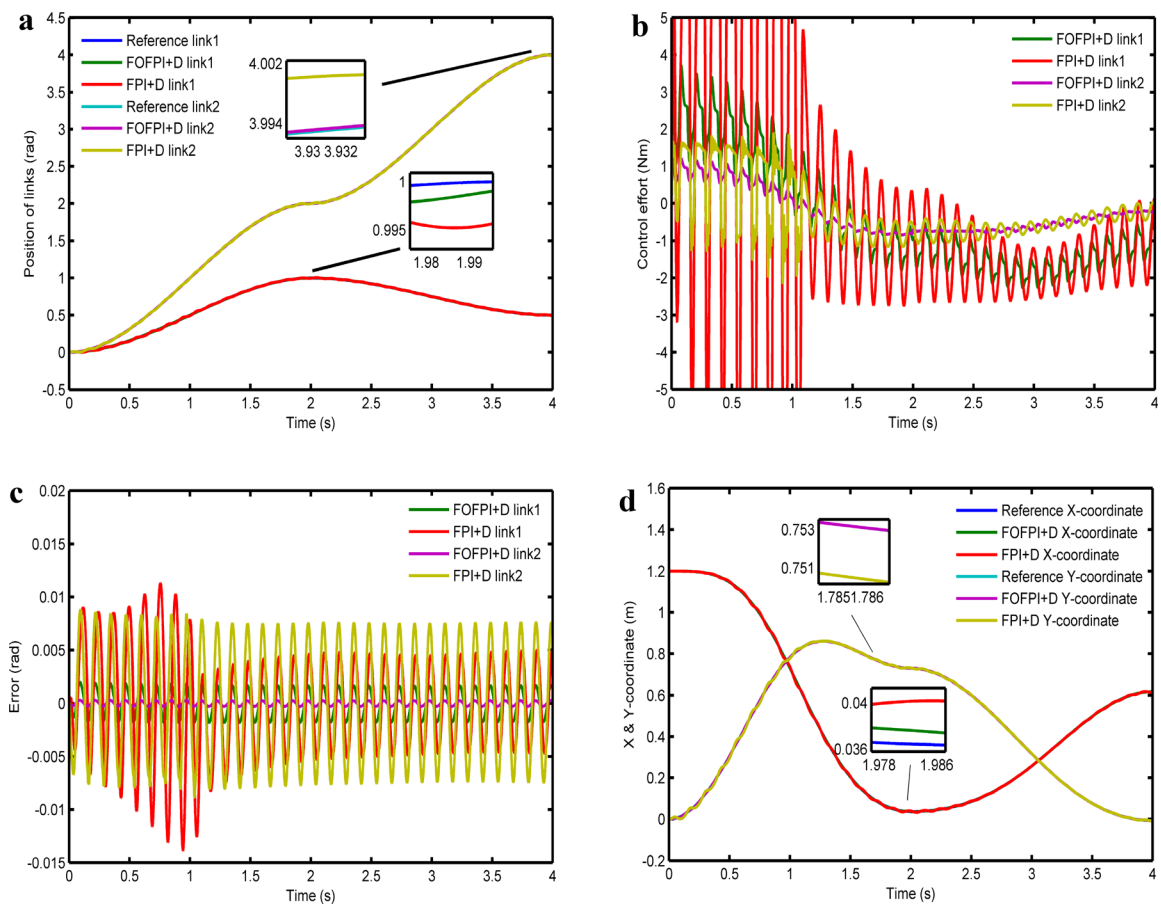


Fig. 13 Tracking response with FOFPI + D and FPI + D controller **a** Links position **b** Control effort **c** Error and **d** End effector position in XY-plane by adding 10Sin50t Nm disturbance in both d1& d2

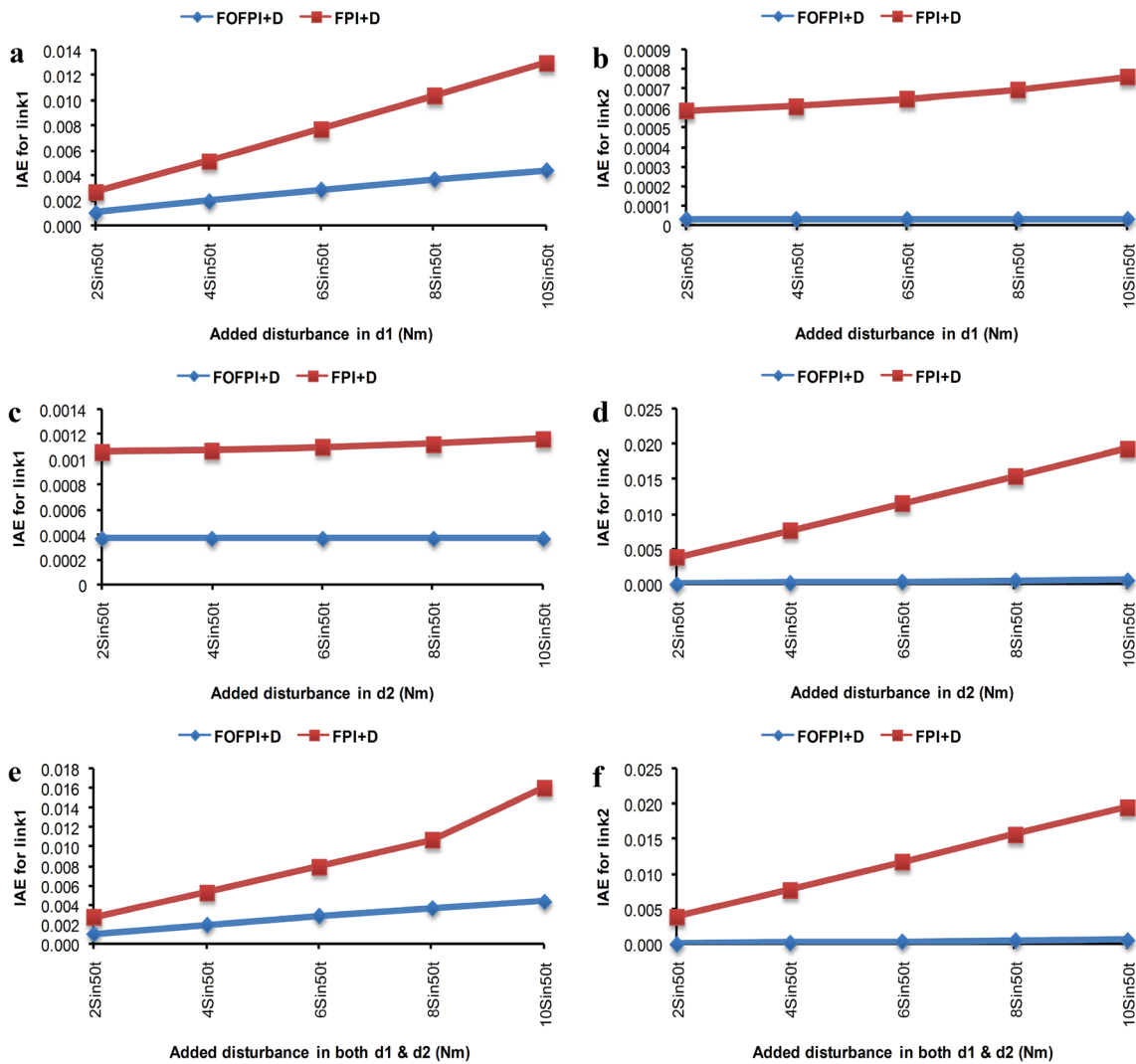


Fig. 14 Variation in IAE by FOFPI + D and FPI + D controller **a** link1 with added disturbance in $d1$ **b** link2 with added disturbance in $d1$ **c** link1 with added disturbance in $d2$ **d** link2 with added disturbance in $d2$ **e** link1 with added disturbance in both $d1$ & $d2$ **f** link2 with added disturbance in both $d1$ & $d2$

4.4.1 Disturbance Rejection with Nominal Parameters of the System

The performance of designed controllers is investigated for disturbance rejection without model uncertainty by introducing a sinusoidal disturbance of different amplitudes (Table 7) for the entire time in $d1$, $d2$, and simultaneously in both $d1$ & $d2$ as shown in Fig. 8. Disturbance rejection response for the case of $10Sin50t$ Nm disturbance is shown in Fig. 13, including tracking response, control effort, position error and XY coordinates of the end effector with time. The IAE from the reference position of link1 and link2 in case of the disturbance rejection is listed in Table 7. For comparative analysis, variations in IAE are plotted and depicted in Fig. 14. It is observed from

graphical and quantitative analysis that the IAE value variations are significantly less for FOFPI + D than for the FPI + D controller. Hence, it can be emphasised that FOFPI + D controller performance is superior to its integer order counterpart in the rejection of disturbance.

4.4.2 Disturbance Rejection with an Uncertain System

In this section, the controller’s intense robustness testing is carried out by incorporating model uncertainty and disturbance. The complete study is accomplished by considering $\pm 35\%$ model uncertainty with the boundary condition of trajectory as $[-4, -1, -7, 5]$ & $[3, 1, 5, -5]$ for link1 and link2, respectively. Moreover, IAE values for added disturbance of $10Sin50t$ Nm in $d1$, $d2$, and both

Table 8 IAE values of FOFPI + D and FPI + D controller by incorporating $\pm 35\%$ parameter uncertainties with added disturbance of $10\sin 50t$ Nm in $d1$, $d2$ and simultaneously in $d1$ & $d2$

Added $\pm 35\%$ model uncertainty and disturbance of $10\sin 50t$ in	IAE by FOFPI + D		IAE by FPI + D	
	Link1 (θ_1)	Link2 (θ_2)	Link1 (θ_1)	Link2 (θ_2)
$d1$	44.85×10^{-4}	31.5×10^{-5}	140.1×10^{-4}	401.4×10^{-5}
$d2$	4.136×10^{-4}	81.8×10^{-5}	19.67×10^{-4}	2536×10^{-5}
Both $d1$ & $d2$	45.36×10^{-4}	83.78×10^{-5}	173.7×10^{-4}	2199×10^{-5}

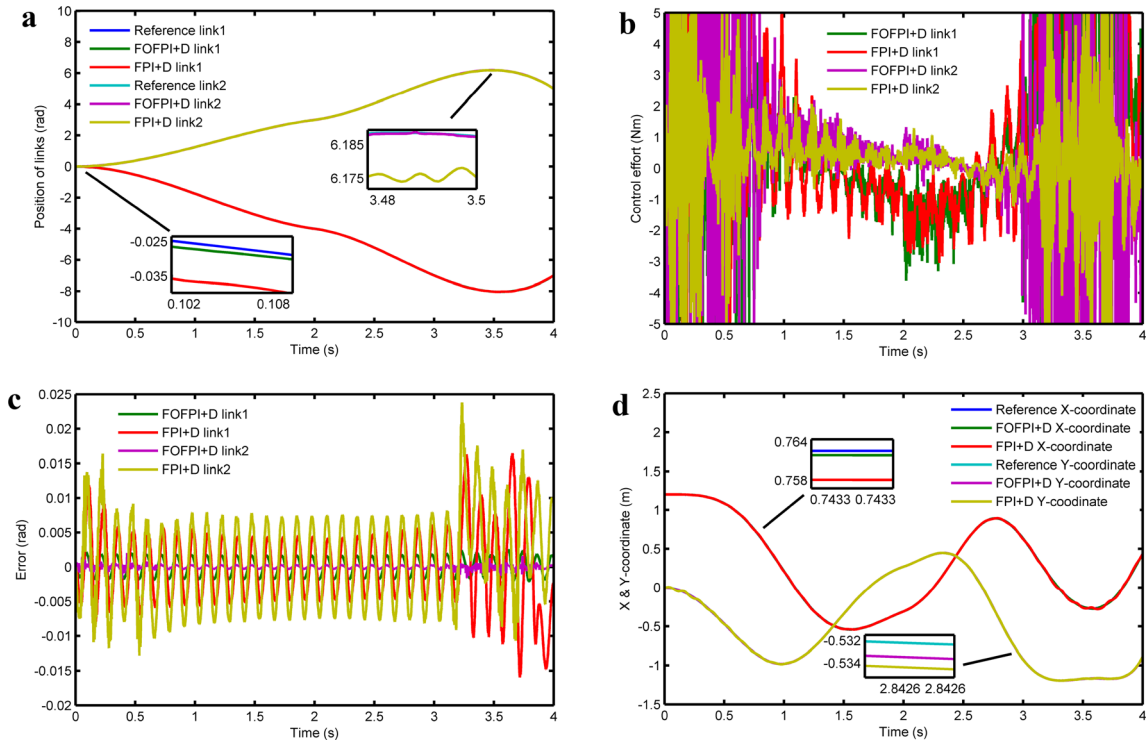


Fig. 15 Tracking response of the system with FOFPI + D and FPI + D controller **a** Links position **b** Control effort **c** Error and **d** End effector position in XY- plane by incorporating $\pm 35\%$ parameter uncertainties with added disturbance of $10\sin 50t$ in both $d1$ & $d2$

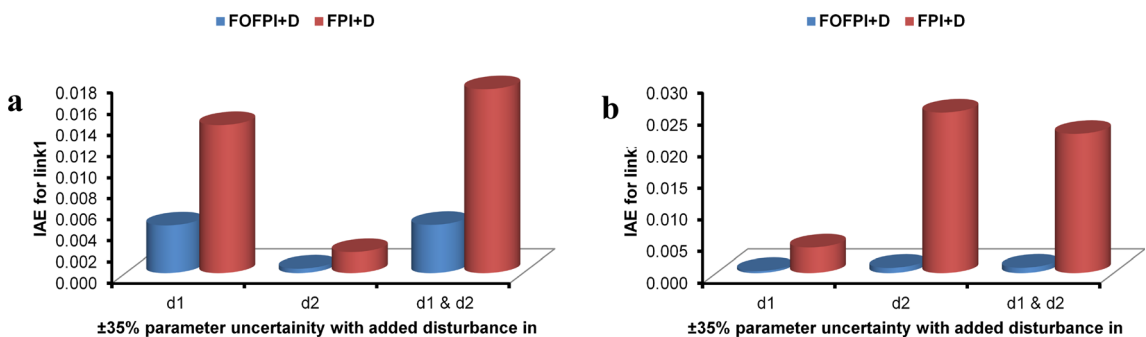


Fig. 16 Quantitative analysis of FOFPI + D and FPI + D controller based on IAE value for **a** link1 and **b** link2 by incorporating $\pm 35\%$ parameter uncertainties with added disturbance of $10\sin 50t$ Nm in $d1$, $d2$ and simultaneously in $d1$ & $d2$

$d1$ & $d2$ simultaneously are recorded in Table 8. The trajectory tracking performance of FOFPI + D and FPI + D controllers and their corresponding variations in torque, position error, and end effector position in XY-plane versus time with added disturbance in both $d1$ & $d2$ are shown in Fig. 15. Further, the bar graphs in Fig. 16 are also used to depict the quantitative performance analysis. It is observed that IAE value of FOFPI + D for link1 and link2 are approximately (33% & 33%), (20% & 0.8%) and (25% & 8%) of FPI + D controller for all the three cases i.e. $d1$, $d2$ and both $d1$ & $d2$ respectively. Thus, the FOFPI + D controller offers robust, effective, and better control than FPI + D.

5 Conclusion

A framework for the fractional fuzzy proportional integral plus derivative (FOFPI + D) controller is demonstrated in this paper. The proposed controller (FOFPI + D) is derived mathematically as a FOFPI and FOFD controller combination. It retains the simple linear structure in PI and D portions but has non-linear gains, enhancing its self-tuning control ability. The analytical formulae for the proposed FOFPI + D controller, fuzzification, rule base setup, and defuzzification are presented. Also, the condition for stability of the closed-loop system using the graphical method is established. Thus, providing assured reliability, stability, and adaptability to the resulting control scheme (FOFPI + D). The proposed controller also exhibits intelligence in making decisions and computations based on a metaheuristic algorithm.

A detailed study of the performance of the proposed FOFPI + D design for the control of a non-linear robotic manipulator is discussed. The controller parameters are optimally tuned through NSGA-II by minimising control signal and error variation. The simulation results show the effectiveness of the FOFPI + D controller for trajectory tracking, robustness against parametric variation, tracking for varying boundary conditions of reference trajectory, and disturbance rejection. Further, the quantitative comparative analysis based on IAE is performed to prove the advantages of AI-based controllers over conventional controllers. The controller could be further advanced by implementing techniques such as neural networks, type 3 fuzzy logic and algorithms.

Author Contributions Methodology, VM; validation, VM and HC; formal analysis, BP and VM; investigation, AR and VM; writing—original draft preparation, VM and BP; writing—review and editing, AR and VS; visualisation, HC and VM; supervision, AR and VS.

Funding Open access funding provided by Manipal Academy of Higher Education, Manipal. The authors declare that no funds, grants, or other support were received during the preparation of this manuscript.

Declarations

Conflict of interest The authors have no relevant financial or non-financial interests to disclose.

Ethical approval This article does not contain any studies with human participants or animals performed by any authors.

Consent to participate Informed consent was obtained from all individual participants included in the study.

Consent for publication Not applicable.

Open Access This article is licensed under a Creative Commons Attribution 4.0 International License, which permits use, sharing, adaptation, distribution and reproduction in any medium or format, as long as you give appropriate credit to the original author(s) and the source, provide a link to the Creative Commons licence, and indicate if changes were made. The images or other third party material in this article are included in the article's Creative Commons licence, unless indicated otherwise in a credit line to the material. If material is not included in the article's Creative Commons licence and your intended use is not permitted by statutory regulation or exceeds the permitted use, you will need to obtain permission directly from the copyright holder. To view a copy of this licence, visit <http://creativecommons.org/licenses/by/4.0/>.

References

1. Kommula, B.N., Kota, V.R.: Design of MFA-PSO based fractional order PID controller for effective torque controlled BLDC motor. *Sustain. Energy Technol. Assess.* **49**, 101644 (2022)
2. Huang, S., et al.: A fixed-time fractional-order sliding mode control strategy for power quality enhancement of PMSG wind turbine. *Int. J. Electr. Power Energy Syst.* **134**, 107354 (2022)
3. Thangam, T., Muthuvel, M.K.: Passive fractional-order proportional-integral-derivative control design of a grid-connected photovoltaic inverter for maximum power point tracking. *Comput. Electr. Eng.* **97**, 107657 (2022)
4. V. P. Shankaran, S. I. Azid, and U. Mehta (2021) "Fractional-order PI plus D controller for second-order integrating plants: stabilisation and tuning method," *ISA Trans.* **129**, 592–604 (2021)
5. L. Liu, D. Xue, and S. Zhang, "General type industrial temperature system control based on fuzzy fractional-order PID controller." *Complex Intell. Syst.* pp. 1–13, 2021.
6. Jain, S., Hote, Y.V.: Order diminution of ITI systems using modified big bang big crunch algorithm and Pade approximation with fractional order controller design. *Int. J. Control Autom. Syst.* **19**(6), 2105–2121 (2021)
7. Guha, D., Roy, P.K., Banerjee, S.: Observer-aided resilient hybrid fractional-order controller for frequency regulation of hybrid power system. *Int. Trans. Electr. Energy Syst.* **31**(9), e13014 (2021)
8. Anjum, Z., Guo, Y.: Finite time fractional-order adaptive backstepping fault tolerant control of robotic manipulator. *Int. J. Control Autom. Syst.* **19**(1), 301–310 (2021)
9. Chhabra, H., Mohan, V., Rani, A., Singh, V.: Robust non-linear fractional order fuzzy PD plus fuzzy I controller applied to

- robotic manipulator. *Neural Comput. Appl.* **32**(7), 2055–2079 (2020)
10. Mohan, V., Chhabra, H., Rani, A., Singh, V.: An expert 2DOF fractional order fuzzy PID controller for non-linear systems. *Neural Comput. Appl.* **31**(8), 4253–4270 (2019)
 11. Mohan, V., Chhabra, H., Rani, A., Singh, V.: Robust self-tuning fractional order PID controller dedicated to non-linear dynamic system. *J. Intell. Fuzzy Syst.* **34**(3), 1467–1478 (2018)
 12. Jajarmi, A., Baleanu, D., Zarghami Vahid, K., Mobayen, S.: A general fractional formulation and tracking control for immunogenic tumor dynamics. *Math. Methods Appl. Sci.* **45**(667), 680 (2022)
 13. Panjwani, B., Mohan, V., Rani, A., Singh, V.: Optimal drug scheduling for cancer chemotherapy using two degree of freedom fractional order PID scheme. *J. Intell. Fuzzy Syst.* **36**(3), 2273–2284 (2019)
 14. Padiachy, V., Mehta, U., Azid, S., Prasad, S., Kumar, R.: Two degree of freedom fractional PI scheme for automatic voltage regulation. *Eng. Sci. Technol. Int. J.* **30**, 101046 (2021)
 15. Y. Pan, Y. Wu, and H.-K. Lam, “Security-based fuzzy control for non-linear networked control systems with DoS attacks via a resilient event-triggered scheme.” *IEEE Trans. Fuzzy Syst.* **30**(10), 4359–4368 (2022)
 16. Pan, Y., Li, Q., Liang, H., Lam, H.-K.: A novel mixed control approach for fuzzy systems via membership functions online learning policy. *IEEE Trans. Fuzzy Syst.* (2021). <https://doi.org/10.1109/TFUZZ.2021.3130201>
 17. Mohammadzadeh, A., Taghavifar, H.: A robust fuzzy control approach for path-following control of autonomous vehicles. *Soft. Comput.* **24**(5), 3223–3235 (2020)
 18. Cao, Y., Raise, A., Mohammadzadeh, A., Rathinasamy, S., Band, S.S., Mosavi, A.: Deep learned recurrent type-3 fuzzy system: application for renewable energy modeling/prediction. *Energy Rep.* **7**, 8115–8127 (2021)
 19. Misir, D., Malki, H.A., Chen, G.: Design and analysis of a fuzzy proportional-integral-derivative controller. *Fuzzy Sets Syst.* **79**(3), 297–314 (1996)
 20. Ying, H., Siler, W., Buckley, J.J.: Fuzzy control theory: a non-linear case. *Automatica* **26**(3), 513–520 (1990)
 21. Malki, H.A., Misir, D., Feigenspan, D., Chen, G.: Fuzzy PID control of a flexible-joint robot arm with uncertainties from time-varying loads. *IEEE Trans. Control Syst. Technol.* **5**(3), 371–378 (1997)
 22. Malki, H.A., Li, H., Chen, G.: New design and stability analysis of fuzzy proportional-derivative control systems. *IEEE Trans. Fuzzy Syst.* **2**(4), 245–254 (1994)
 23. Sooraksa, P., Chen, G.: Mathematical modeling and fuzzy control of a flexible-link robot arm. *Math. Comput. Model.* **27**(6), 73–93 (1998)
 24. Li, W., Chang, X., Wahl, F.M., Farrell, J.: Tracking control of a manipulator under uncertainty by FUZZY P+ ID controller. *Fuzzy Sets Syst.* **122**(1), 125–137 (2001)
 25. Er, M.J., Sun, Y.L.: Hybrid fuzzy proportional-integral plus conventional derivative control of linear and non-linear systems. *IEEE Trans. Industr. Electron.* **48**(6), 1109–1117 (2001)
 26. Tang, W., Chen, G., Lu, R.: A modified fuzzy PI controller for a flexible-joint robot arm with uncertainties. *Fuzzy Sets Syst.* **118**(1), 109–119 (2001)
 27. Tang, K.-S., Man, K.F., Chen, G., Kwong, S.: An optimal fuzzy PID controller. *IEEE Trans. Industr. Electron.* **48**(4), 757–765 (2001)
 28. Chen, G., Pham, T.T.: Introduction to fuzzy sets, fuzzy logic, and fuzzy control systems. CRC Press, Boca Raton (2000)
 29. Das, S., Pan, I., Das, S.: Performance comparison of optimal fractional order hybrid fuzzy PID controllers for handling oscillatory fractional order processes with dead time. *ISA Trans.* **52**(4), 550–566 (2013)
 30. Das, S., Pan, I., Das, S.: Fractional order fuzzy control of nuclear reactor power with thermal-hydraulic effects in the presence of random network induced delay and sensor noise having long range dependence. *Energy Convers. Manag.* **68**, 200–218 (2013)
 31. Das, S., Pan, I., Das, S., Gupta, A.: A novel fractional order fuzzy PID controller and its optimal time domain tuning based on integral performance indices. *Eng. Appl. Artif. Intell.* **25**(2), 430–442 (2012)
 32. Jesus, I.S., Barbosa, R.S.: Genetic optimisation of fuzzy fractional PD+ I controllers. *ISA Trans.* **57**, 220–230 (2015)
 33. Mohammadikia, R., Aliasghary, M.: A fractional order fuzzy PID for load frequency control of four-area interconnected power system using biogeography-based optimisation. *Int. Trans. Electr. Energy Syst.* **29**(2), e2735 (2019)
 34. Zamani, A.-A., Tavakoli, S., Etedali, S., Sadeghi, J.: Online tuning of fractional order fuzzy PID controller in smart seismic isolated structures. *Bull. Earthq. Eng.* **16**(7), 3153–3170 (2018)
 35. Patel, N.C., Sahu, B.K., Bagarty, D.P., Das, P., Debnath, M.K.: A novel application of ALO-based fractional order fuzzy PID controller for AGC of power system with diverse sources of generation. *Int. J. Electr. Eng. Educ.* **58**(2), 465–487 (2021)
 36. Zhang, F., Yang, C., Zhou, X., Zhu, H.: Fractional order fuzzy PID optimal control in copper removal process of zinc hydrometallurgy. *Hydrometallurgy* **178**, 60–76 (2018)
 37. Pan, I., Das, S.: Fractional order fuzzy control of hybrid power system with renewable generation using chaotic PSO. *ISA Trans.* **62**, 19–29 (2016)
 38. Mohan, V., Pachauri, N., Panjwani, B., Kamath, D.V.: A novel cascaded fractional fuzzy approach for control of fermentation process. *Bioresour. Technol.* **357**, 127377 (2022)
 39. J. Jantzen “Tuning of fuzzy PID controllers,” *Technical University of Denmark, Department of Automation, Bldg.* vol. 326, (1998).
 40. Goodrich, C., Peterson, A.C.: Discrete fractional calculus. Springer, New York (2015)
 41. Lubich, C.: Discretized fractional calculus. *SIAM J. Math. Anal.* **17**(3), 704–719 (1986)
 42. Oldham, K., Spanier, J.: The fractional calculus theory and applications of differentiation and integration to arbitrary order. Elsevier, Amsterdam (1974)
 43. Y. Chen, I. Petras, and D. Xue (2009) “Fractional order control-a tutorial.” In: *2009 American control conference: IEEE*, pp. 1397–1411.
 44. Driankov, D., Hellendoorn, H., Reinfrank, M.: An introduction to fuzzy control. Springer Science & Business Media, New York (2013)
 45. Zadeh, L.A.: Fuzzy sets. *Inf. Control* **8**(3), 338–353 (1965)
 46. Deb, K., Pratap, A., Agarwal, S., Meyarivan, T.: A fast and elitist multiobjective genetic algorithm: NSGA-II. *IEEE Trans. Evol. Comput.* **6**(2), 182–197 (2002)
 47. Chhabra, H., Mohan, V., Rani, A., Singh, V.: Trajectory tracking of Maryland manipulator using linguistic Lyapunov fuzzy controller. *J. Intell. Fuzzy Syst.* **36**(3), 2195–2205 (2019)
 48. Panjwani, B., Singh, V., Rani, A., Mohan, V.: Optimum multi-drug regime for compartment model of tumour: cell-cycle-specific dynamics in the presence of resistance. *J. Pharmacokinetic Pharmacodyn.* **48**(4), 543–562 (2021)
 49. J. J. Craig, *Introduction to robotics: mechanics and control, 3/E*. Pearson Education India, 2005
 50. Ayala, H.V.H., dos Santos Coelho, L.: Tuning of PID controller based on a multiobjective genetic algorithm applied to a robotic manipulator. *Exp. Syst. Appl.* **39**(10), 8968–8974 (2012)



Vijay Mohan is working as an Assistant Professor in Department of Mechatronics, Manipal Institute of Technology, Udipi India. He has done his B.Tech. (Electronics & communication) from UPTU, Lucknow, Uttar Pradesh, M. Tech. (Control & Instrumentation) from NIT, Jalandhar, Punjab, and Ph.D. (Instrumentation and control) from Netaji subhas institute of technology, University of Delhi, New Delhi. He has over 8 years

of teaching and research experience in institutes of repute. He has published several papers in journals, conference proceedings and book chapters. He has published 3 Indian patents and 5 International patents. His area of research includes Artificial Intelligence, IOT, Metaheuristics, Machine Learning, Drug scheduling, Control Engineering and Process control.



Bharti Panjwani completed her Ph.D. from Netaji Subhas Institute of Technology, University of Delhi, New Delhi. She has done her B.E. in the field of Electronics & Telecommunication) from CSVTU, Chhattisgarh, India, and M.Tech. with specialization in control and instrumentation engineering from National Institute of Technology, Jalandhar, Punjab, India. She has over 6 years of teaching and research experience from reputed institutes of

India. Her current research focus is on optimization of drug schedules in chemotherapy. She has published several papers in journals and conference proceedings. Her area of research includes IOT, control engineering, neural networks, optimization techniques, biomedical engineering, drug scheduling, artificial intelligence.



Himanshu Chhabra received his B.Tech degree in Electronics & Communication Engineering from U.P. Technical University, Lucknow in 2012 and M.Tech degree in Instrumentation and Control Engineering from National Institute of Technology Jalandhar in 2014. He received his PhD degree from Faculty of Technology, University of Delhi, New Delhi in 2021. Currently He is working as assistant professor in Mechatronics Department, Parul

University Vadodara, Gujarat. His research interest includes

Biomedical signal processing, Optimization technique, Robotics, Machine learning and Artificial intelligent control.



Asha Rani received her B.Tech. in Electrical Engineering from Regional Engineering College (Now NIT), Hamirpur, Himachal Pradesh in 1998. She received M.E. degree in Electrical Engineering from IIT Roorkee in 2000 and Ph.D. in 2013 from University of Delhi, Delhi. She joined as lecturer in Instrumentation and Control Engineering Division at Netaji Subhas University of Technology, New Delhi in 2001 and currently she is a professor in

the organisation. She has published many papers in international journals and conferences. More than 28 M.Tech. and 6 Ph.D. thesis are completed under her guidance. Currently 3 Ph.D. students are working under her supervision. Her areas of research are Renewable Energy, Intelligent Control, Adaptive Control, Softcomputing based Adaptive Control, Biomedical Signal Processing and Robotic manipulator. She is the senior member of IEEE and IETE.



Vijander Singh received his B. Tech in Electrical Engineering from G.B. Pant University of Agriculture and Technology in Uttarakhand in 1995. He received M.E. degree in Electrical Engineering in 2000 and Ph. D in Electrical Engineering in 2007 from IIT Roorkee. He has published more than 100 papers in international journals and conferences. He is the reviewer of many international journals and has chaired a number of international confer-

ences. He has delivered many expert lectures at different engineering institutes. More than 30 M.Tech theses and 10 Ph.D. theses have been completed under his guidance. Currently 4 Ph.D. students are working with him. He has received best paper awards for a number of papers and Gauri Memorial award in 2019 for best paper of IET journal. He is working as Professor in the Department of Instrumentation and Control Engineering at Netaji Subhas University of Technology. He has the responsibilities of Dean Student Welfare, Dean Faculty of Management Studies, and Dean Faculty of Architecture and Design. He is the member of IEEE and his areas of research are Process control, Biomedical Instrumentation, Artificial Intelligence and Image Processing.